INFORMATION TO USERS

This reproduction was made from a copy of a document sent to us for microfilming. While the most advanced technology has been used to photograph and reproduce this document, the quality of the reproduction is heavily dependent upon the quality of the material submitted.

The following explanation of techniques is provided to help clarify markings or notations which may appear on this reproduction.

1. The sign or "target" for pages apparently lacking from the document photographed is "Missing Page(s)". If it was possible to obtain the missing page(s) or section, they are spliced into the film along with adjacent pages. This may have necessitated cutting through an image and duplicating adjacent pages to assure complete continuity.

2. When an image on the film is obliterated with a round black mark, it is an indication of either blurred copy because of movement during exposure, duplicate copy, or copyrighted materials that should not have been filmed. For blurred pages, a good image of the page can be found in the adjacent frame. If copyrighted materials were deleted, a target note will appear listing the pages in the adjacent frame.

3. When a map, drawing or chart, etc., is part of the material being photographed, a definite method of "sectioning" the material has been followed. It is customary to begin filming at the upper left hand corner of a large sheet and to continue from left to right in equal sections with small overlaps. If necessary, sectioning is continued again—beginning below the first row and continuing on until complete.

4. For illustrations that cannot be satisfactorily reproduced by xerographic means, photographic prints can be purchased at additional cost and inserted into your xerographic copy. These prints are available upon request from the Dissertations Customer Services Department.

5. Some pages in any document may have indistinct print. In all cases the best available copy has been filmed.

University Microfilms International
300 N. Zeeb Road
Ann Arbor, MI 48106

MacFarlane, Joseph John

THEORETICAL PREDICTIONS FOR THE PHASE STABILITY OF DENSE BINARY MIXTURES

The University of Arizona PH.D. 1983

THEORETICAL PREDICTIONS FOR THE PHASE STABILITY OF DENSE BINARY MIXTURES

by

Joseph John MacFarlane

A Dissertation Submitted to the Faculty of the

DEPARTMENT OF PLANETARY SCIENCES

In Partial Fulfillment of the Requirements
For the Degree of

DOCTOR OF PHILOSOPHY

In the Graduate College

THE UNIVERSITY OF ARIZONA

1 9 8 3

THE UNIVERSITY OF ARIZONA
GRADUATE COLLEGE

As members of the Final Examination Committee, we certify that we have read the dissertation prepared by Joseph John MacFarlane

entitled Theoretical Predictions for the Phase Stability of Dense Binary Mixtures

and recommend that it be accepted as fulfilling the dissertation requirement for the Degree of Doctor of Philosophy.

W. B. Hubbard	8/17/83 Date
Michael J. Drake	8/17/83 Date
J. R. Johnson	8/17/83 Date
Michael Banfield	8/17/83 Date
Neil Gehrels	17 Aug 83 Date

Final approval and acceptance of this dissertation is contingent upon the candidate's submission of the final copy of the dissertation to the Graduate College.

I hereby certify that I have read this dissertation prepared under my direction and recommend that it be accepted as fulfilling the dissertation requirement.

W. B. Hubbard	8/17/83
Dissertation Director	Date

STATEMENT BY AUTHOR

This dissertation has been submitted in partial fulfillment of requirements for an advanced degree at The University of Arizona and is deposited in the University Library to be made available to borrowers under rules of the Library.

Brief quotations from this dissertation are allowable without special permission, provided that accurate acknowledgment of source is made. Requests for permission for extended quotation from or reproduction of this manuscript in whole or in part may be granted by the head of the major department or the Dean of the Graduate College when in his judgment the proposed use of the material is in the interests of scholarship. In all other instances, however, permission must be obtained from the author.

SIGNED: Joseph J. MacFarlane

ACKNOWLEDGEMENTS

I wish to thank my adviser, Bill Hubbard, for suggesting this project, and for his guidance throughout the past 5 years. It has been a pleasure working with him. I also wish to acknowledge my fellow graduate students and other friends I have made during my stay in Tucson; especially Bill Merline, who has been a constant source of intellectual and logical discussion, as well as a good drinking buddy. Finally, special appreciation is felt for my parents, and Jane, Julie, Jim^2, and Jeff. Their moral support and friendship throughout the past 5 years has been invaluable.

TABLE OF CONTENTS

LIST OF TABLES

LIST OF ILLUSTRATIONS

ABSTRACT

A new approach is developed for evaluating the mixing properties of binary solutions at high pressure. This involves solving Poisson's equation throughout three-dimensional cubic lattices, consistent with Thomas-Fermi-Dirac (TFD) theory. Zero temperature calculations are carried out for a variety of compositions and crystal structures in 3 pressure groups relevant to Jovian planetary interiors. Pseudopotentials based on the two-component-plasma model (with a uniform electron background) are fitted to the solid-state results, and are then used in liquid-state calculations using hard-sphere perturbation theory.

TFD results for H-He solutions find critical temperatures (above which all compositions are soluble) to be $\sim$ 0, 500, and 1500 ^{o}K at pressures of 10, 100, and 1000 Mbar, respectively. These temperatures are much lower than those obtained using free electron perturbation theory, where $T_{crit} \sim$ 10,000 ^{o}K at 10 Mbar. Thus, unlike the perturbation theory results, the TFD results predict that helium should be soluble in metallic hydrogen in the deep interiors of both Jupiter and Saturn, and our calculations give an indication of the degree of model-dependence in computing high pressure mixing

properties. In addition, TFD calculations for H-C and H-O solutions find phase separation temperatures to be $\lesssim 10^4$ ^oK for pressures $\lesssim 10^3$ Mbar. These temperatures are considerably lower than those found assuming a uniform electron distribution (where $T_{crit} \gtrsim 10^5$ ^oK), and suggest that H-C and H-O solutions should also be miscible in the metallic zones of Jupiter and Saturn.

CHAPTER 1

INTRODUCTION

Determining the physical properties of mixtures at high pressures is essential if one wishes to predict the internal structures and chemical distributions of astrophysical objects. For most stars, hydrogen and helium are by far the most abundant chemical species. But for the planets of our solar system, determining the properties of silicate-type materials (for the inner terrestrial planets) and carbon, nitrogen, and oxygen compounds (for the outer Jovian planets) becomes important. For example, carbon, nitrogen, and oxygen may represent as much as two-thirds of the total mass of Uranus and Neptune (Hubbard and MacFarlane, 1980). Therefore, it is of interest to predict the physical properties of not only H-He solutions, but also mixtures containing C, N, and O.

During the past 10 to 15 years, broadband infrared observations have found that Jupiter, Saturn, and Neptune are all reradiating about twice as much energy as they receive from the Sun (Armstrong, et al., 1972; Low, 1966; Lowenstein, et al., 1977). But large excess luminosities are not unexpected for the giant planets because it is expected that their early internal temperatures were considerably higher that their present internal temperatures. The excess energy outputs of Jupiter (Graboske, et al., 1975) and Neptune

(Hubbard and MacFarlane, 1980) can in fact be fully explained by the thermal energy trapped in the interior of these planets at the time of their formations. However, evolutionary calculations for Saturn (Pollack, et al., 1977) find that its current energy output is too high to be explained by this simple cooling model, and therefore needs an additional internal energy source which has been active over the past two billion years. It has been suggested (Smoluchowski, 1967; Salpeter, 1973) that at low enough temperatures, helium may become immiscible in metallic hydrogen. If this does occur, the denser He-rich phase could form droplets and sink toward the core of Saturn, liberating gravitational energy (Stevenson and Salpeter, 1977). So it is very important to determine not only the bulk thermodynamic properties of relevant mixtures (such as the total energies and pressures), but also the mixing properties of these solutions.

For relatively cool astrophysical objects, such as white dwarfs and giant planets, temperatures are much lower than the electron degeneracy temperatures (although still above the melting points of the majority of their chemical constituents) and pressures are typically in the multimegabar range. At these pressures ($\gtrsim$ 1 Mbar), the kinetic energy of electrons exceeds their binding energy to protons, and hydrogen becomes pressure-ionized (commonly referred to as "liquid metallic hydrogen"). In fact, in the high pressure limit, all species can be regarded as fully pressure-ionized. Under such conditions, the electrons are stripped from their nuclei and the electronic wave functions are plane wave states, so that the system

behaves like a plasma of positively-charged point ions on a uniform negative background. For this case, the total energy for a given ion configuration is readily calculated. As the pressure is reduced from this asymptotic limit, however, deviations for the electronic wave functions from plane wave states must be taken into account, and it becomes necessary to make approximations.

The method commonly used to study the properties of H-He fluids is free electron perturbation theory. Here, one assumes that the electrostatic potential is sufficiently weak that the electronic wave functions can be treated as a small perturbation from plane wave states. Hubbard (1972) and Stevenson (1975) have shown that hydrogen can be accurately treated with this approach at pressures relevant to the deep interiors of giant planets ($\sim$ 1 to 10^2 Mbar). However, helium does not become "metallic" at pressures below $\sim$ 100 Mbar (Young, et al., 1981), and therefore it is questionable whether helium can be accurately modelled using this approach. For materials of higher atomic number, this perturbation method should at the minimum require the evaluation of a large number of terms in the perturbation expansion.

The first study to assess the phase stability regions of fluid hydrogen-helium mixtures in this temperature and pressure range was carried out by Stevenson (1975). In his investigation, he employed hard-sphere perturbation theory to simulate the properties of a fluid, and used linear response theory to model the response of the electron gas to the electrostatic potential (also the free electron

perturbation expansion was calculated to second-order). The principal advantage of the perturbation approach is that the pair-potentials are easily evaluated, and can therefore by used for computing the properties of liquid mixtures. However, since the method assumes small perturbations from plane wave states, it is necessary to determine how rapidly the expansion converges (if at all) in the pressure range of interest for giant planet interiors. Errors which are considered acceptably small for such thermodynamic properties as the total energy or pressure, may be very large for other quantities, such as mixing energies.

In this study, a model is developed for calculating the mixing properties of solutions based on Thomas-Fermi-Dirac [TFD] theory. TFD theory is a semi-classical model which treats the electrons of a given atomic configuration as being locally free and obeying Fermi statistics (Thomas, 1927; Fermi, 1928). The electron density is then determined at each point by the self-consistent electrostatic potential. The limitations of TFD theory (discussed in Chapter 2) are substantial, but the theory does provide an alternative, non-linear approach for assessing the thermodynamic properties of mixtures at high pressures. In addition, the TFD model becomes more useful for atoms of higher atomic number Z, where free electron perturbation theory breaks down. TFD equations of state for high-Z materials are in qualitative agreement with high pressure data in the megabar pressure range, and TFD theory predicts the correct pressure-density relation as the pressure goes to infinity (Salpeter and Zapolsky, 1967).

In the usual one-dimensional application of TFD theory, atoms are assumed to be spherically symmetric, occupying individual, overall neutral Wigner-Seitz cells. Neighboring cells do not interact. The pressure-volume relations of mixtures are found by adjusting the volumes of each of the cells so that the pressure (given by the pressure of an ideal Fermi gas of electrons at the surface of each cell) is the same for all atoms. Because the deviations from ideal mixing are zero by definition, no information on the mixing properties (e.g., phase separation behavior) can be obtained.

In Chapter 2, a numerical procedure is presented for solving the TFD equation in three dimensions for crystalline structures containing a given number of ions of various values of Z at specified lattice sites. After solving the three-dimensional TFD equation for the electron distribution in a crystal, relevant zero-temperature thermodynamic properties are calculated, and ultimately the deviations from ideal mixing are computed. Because the mixing energies are so small ($\lesssim$ 1% of the total energy), the integral and differential equations must be evaluated with a high degree of numerical accuracy.

In Chapter 3, the results for the zero temperature calculations are presented. Results for the hydrogen-helium system are compared with those from perturbation theory calculations. Even for H-He solutions, the differences between TFD theory and perturbation theory are significant. Although both theories are in qualitative agreement in predicting bulk thermodynamic properties (e.g., total energy or pressure), small but very significant

differences arise in the mixing energies, leading to very different predictions for the phase stability of H-He solutions.

In Chapter 4, pseudopotentials are developed for the TFD models based on the Ewald potential for two-component-plasmas. These are found by fitting the solid-state TFD data to a model free energy, with effective ion charges (which are smaller than the actual ion charges because of screening effects) and an additional structure-independent energy term. This pseudopotential is then used in liquid-state calculations using hard-sphere perturbation theory. With this approach, we are able to calculate the mixing properties of fluid systems based on TFD theory, including the phase separation regions.

In Chapter 5, the free energy formalism is developed for the liquid-state calculations based on hard-sphere perturbation theory. In Chapter 6, the results for the phase separation temperatures are presented. Also, the TFD results of other equilibrium properties are compared with those from other models. Finally, in Chapter 7, the validity of these results is discussed, as well as the implications they may have for the chemical distributions and energy sources in planetary interiors.

CHAPTER 2

SOLID-STATE THOMAS-FERMI-DIRAC MODEL

TFD Theory

Thomas-Fermi-Dirac theory begins by assuming that the electrostatic potential varies so slowly throughout the electron gas that the electronic wave functions may be described locally as plane waves. This assumption of course breaks down in the vicinity of the nucleus where the electrostatic potential varies quite rapidly, and it becomes less valid for atoms of smaller atomic number. As a result, the TFD model permits strong response of the electron gas to the electrostatic potential and the electron cloud is too tightly bound to the nucleus. In addition, the electron distribution is smoothed out in the statistical averaging process so that the TFD model gives no indication of shell structure, whereas relatively more elaborate calculations, such as those using a Hartree approach, do exhibit shell structure for many-electron atoms (see e.g., Mizushima, 1970). Therefore, the TFD model should be regarded as a somewhat crude model for calculating the electron distribution for an atom.

But using Thomas-Fermi-Dirac theory does provide significant practical advantages. Because we are interested in assessing the mixing properties of binary systems, and therefore must solve the three-dimensional problem, computational complexities are inherent to

the calculation. Typical mixing energies for the solutions discussed below represent only $\sim$ 1 % of the total energy of the system. This requires that the total energies be evaluated with a numerical accuracy of $\lesssim$ 1 part in 10^3. Therefore, it is of considerable advantage to use an approach which predicts a relatively smooth charge distribution, as well as permitting the electron distributions to be evaluated in three dimensions relatively easily.

In order to evaluate the zero temperature mixing properties, one must first compute the electron distribution for a specified ion configuration. To do this, we must solve Poisson's equation in three dimensions, consistent with Thomas-Fermi-Dirac theory. In the absence of an external field, the chemical potential for a Fermi gas of electrons on a uniform neutralizing background, at zero temperature, can be expanded in the form:

$$\mu_e = \frac{1}{2}(3\pi^2)^{2/3}\, n_e^{2/3} - (3/\pi)^{1/3}\, n_e^{1/3}, \qquad (2.1)$$

where n_e is the number density of electrons, and all quantities here and in following expressions are given in atomic units (au). The atomic unit of volume is a_0^3 (a_0 = Bohr radius), the atomic unit of energy is e^2/a_0 = 27.2 eV (e = electron charge), and the atomic unit of pressure is e^2/a_0^4 = 294.2 Mbar. The first term on the right hand side is the contribution from the free-electron kinetic energy, while the second term arises from the first-order exchange energy between electrons. In the presence of the electric field, which results from the fact that the ions are essentially point charges, the total

electron chemical potential becomes:

$$\mu = \mu_e - \phi, \tag{2.2}$$

where ϕ is the electrostatic potential produced by the electrons and ions. We now utilize the equilibrium requirement that the total electron chemical potential remain constant throughout the electron gas (Landau and Lifshitz, 1969), and apply Poisson's equation to get:

$$\nabla^2 X(r) = 8\pi^3 n_e(r) = (8/3\pi^2)\,(1+X^{1/2})^3, \tag{2.3}$$

where r is the position vector, and

$$X(r) = 1 + 2\pi^2\,[\mu + \phi(r)]. \tag{2.4}$$

Equation (2.3) is the three-dimensional TFD equation, which is nonlinear and is solved numerically to get the electron distribution.

Method of Calculation

For the zero temperature calculations, the ion configurations were chosen to be either a body-centered-cubic (bcc), face-centered-cubic (fcc), or simple cubic (sc) lattice. There are a number of reasons for using these structures: (1) all are Bravais lattices, enabling all ions to be placed at one of our evenly spaced mesh points; (2) all are symmetric with respect to the coordinate axes, necessitating the computation of the electron distribution for only one octant of the unit cell; and (3) their total energies are relatively low and therefore should give reasonable estimates of the non-ideality of a mixture in its preferred configuration.

The solution of the TFD equation is carried out over a unit cell with edge length L containing N ions with charges Z_i (i =

1,2,...,N). We require the unit cell to be identically repeated in all directions, so that $\phi(\mathbf{r})$ [and therefore $n_e(\mathbf{r})$ and $X(\mathbf{r})$] obeys periodic boundary conditions:

$$\phi(\mathbf{r}) = \phi(\mathbf{r} + n\mathbf{L}), \tag{2.5}$$

where $\mathbf{n}$ is a vector with integer components. We also have the boundary conditions:

$$\int_V d^3r\, n_e(\mathbf{r}) = \sum_{i=1}^{N} Z_i \tag{2.6}$$

and

$$\mu_i = \mu_j, \quad i,j = 1,2,\ldots,N, \quad i \neq j, \tag{2.7}$$

where $V = L^3$ is the volume of the unit cell and μ_i is the electron chemical potential evaluated at the i^{th} ion. Equation (2.6) is obviously the mathematical expression for charge neutrality and equation (2.7) requires the electron chemical potential to have the same value at all ion sites.

Since $\phi(\mathbf{r})$ becomes unbounded near each ion, the solution of the TFD equation near ions must be handled in a special manner. Noting that $\phi(\mathbf{r})$ and $n_e(\mathbf{r})$ must become spherically symmetric in the vicinity of ions, we center each ion in a small cubic subcell of volume $V_{sc} = L_{sc}^3$, and assume the electron distribution to be radially symmetric within this region. (Solutions for the mixtures discussed below were carried out with $L/L_{sc} = 40/7$ and verified to be insensitive to the choice of L_{sc}.) The solution within the subcells is found using the one-dimensional version of the TFD equation, with

boundary conditions determined in a self-consistent manner from the full three-dimensional solution in the remainder of the unit cell. Using a change of variables, the usual one-dimensional TFD equation is written:

$$\frac{1}{x}\frac{d^2z}{dx^2} = [\varepsilon + (z/x)^{1/2}]^3, \tag{2.8}$$

where

$$x = 2\,Z^{1/3}\,(4/3\pi)^{2/3}\,q,$$

$$z = q\,X(q)/(2\,\pi^2 Z),$$

and

$$\varepsilon = (3/32\,\pi^2 Z^2)^{1/3}.$$

Here $q = r - r_i$ is the radial distance from an ion and Z is the charge of the ion. The electrostatic potential must approach the unscreened Coulomb potential of the ion as $x \to 0$, so that

$$\lim_{x\to 0} z(x) = 1. \tag{2.9}$$

Since eq. (2.8) is a second-order differential equation, a second boundary condition is needed to specify the solution. This boundary condition is the value of $(dz/dx)_{x=0}$ at each of the N ions, which we will momentarily find using eq. (2.7). We then have N constraining equations [equations (2.6) and (2.7)] in N unknowns, which we solve by iteration.

Assuming a value for $(dz/dx)_{x=0}$ at each ion, we solve equation (2.8) in each subcell using the Runge-Kutta method for second-order differential equations (Abramowitz and Stegun, 1965) [using the formula accurate to $\sim h^3$, a step length of $h = L_{sc}/200$ provides sufficient accuracy for the problem]. The spherically-symmetric

solution for X(q) centered on each ion is then used to provide values for X(r) at the three-dimensional mesh points inside each subcell. We then solve Poisson's equation [eq. (2.3)] on the remainder of the mesh points in the unit cell. Beginning with a uniform electron density throughout the unit cell (excluding of course the subcells), a new value for the electron density at each mesh point is found by solving for X(r) on the right hand side of eq. (2.3). Numerical differentiation using 5 mesh points in each coordinate direction gives sufficient accuracy in evaluating the Laplacian on the left hand side of eq. (2.3). The procedure is repeated until a stable X(r) is found. Successive overrelaxation is employed to accelerate convergence.

After the electron distribution in the unit cell is found, the boundary condition equations must be updated. Numerical integration of the charge balance equation is straightforward. Evaluation of the electron chemical potential at each ion is more complicated because it is determined by the long-range Coulomb potential. Considering eq. (2.4) in the vicinity of an ion, multiplying it by q, and then differentiating with respect to q, one finds:

$$\mu_i = Z_i \, (dz/dq)_{q=0} - 1/(2\pi^2) - \phi_o^i, \tag{2.10}$$

where

$$\phi_o^i = \sum_{j \neq i}^{\text{all space}} Z_j / \, |r_j - r_i| - \int_{\text{all space}} d^3r \; n_e(r) / \, |r - r_i| \, . \tag{2.11}$$

Here ϕ_o^i is the electrostatic potential evaluated at the i^{th} ion with the infinite self-potential of the ion subtracted out. The sum and

integral in eq. (2.11) must be taken out to infinity, including all charges in image cells as well as in the unit cell. To evaluate ϕ_o^i, we take advantage of the periodic boundary conditions and expand the charge density and the potential in a Fourier series:

$$n(\mathbf{r}) = V^{-1} \sum_{\mathbf{k}} n_{\mathbf{k}} \exp(i\mathbf{k}\cdot\mathbf{r}),$$

$$\phi(\mathbf{r}) = V^{-1} \sum_{\mathbf{k}} \phi_{\mathbf{k}} \exp(i\mathbf{k}\cdot\mathbf{r}), \qquad (2.12)$$

where the wave vector $\mathbf{k} = 2\pi \mathbf{n}/L$. Writing the charge density as:

$$n(\mathbf{r}) = \sum_{i=1}^{N} Z_i \, \delta(\mathbf{r}-\mathbf{r}_i) - n_e^o - \delta n_e(\mathbf{r}), \qquad (2.13)$$

where n_e^o is the average electron density and $\delta n_e(\mathbf{r})$ is the fluctuation of the local electron density with respect to the average value, we see that the Fourier coefficients for the charge density become:

$$n_{\mathbf{k}} = \int_V d^3r \; n(\mathbf{r}) \exp(-i\mathbf{k}\cdot\mathbf{r})$$

$$= \sum_{i=1}^{N} Z_i \exp(-i\mathbf{k}\cdot\mathbf{r}_i) - \int_V d^3r \; \delta n_e(\mathbf{r}) \exp(-i\mathbf{k}\cdot\mathbf{r}); \quad \mathbf{k} \neq 0. \qquad (2.14)$$

Charge neutrality requires the $\mathbf{k} = 0$ term to be zero. Applying Poisson's equation to eq. (2.13), the potential becomes:

$$\phi(\mathbf{r}) = (4\pi/V) \sum_{i=1}^{N} Z_i \sum_{\mathbf{k}}{}' k^{-2} \exp[i\mathbf{k}\cdot(\mathbf{r}-\mathbf{r}_i)]$$

$$- \int_V d^3r' \; \delta n_e(\mathbf{r}') \sum_{\mathbf{k}}{}' k^{-2} \exp[i\mathbf{k}\cdot(\mathbf{r}-\mathbf{r}')] \;, \qquad (2.15)$$

where the prime on the summation indicates the $\mathbf{k} = 0$ term is excluded.

We now employ the trick originally used by Ewald (1921) and described in Brush, et al. (1966), which permits rapid evaluation of the sums in eq. (2.15). Let

$$U(q) = (4\pi/V) \sum_{k}{}' k^{-2} \exp(ik\cdot q)$$

$$= q^{-1} \operatorname{erfc}(\pi^{1/2} q/L) - \frac{1}{L}$$

$$+ \frac{1}{L} \sum_{n}{}' (\pi n^2)^{-1} \exp[-\pi n^2 + i(2\pi n/L)\cdot q]$$

$$+ \sum_{n}{}' |nL - q|^{-1} \operatorname{erfc}[\pi^{1/2} |n-(q/L)|], \qquad (2.16)$$

where $\operatorname{erfc}(y) = 1 - \operatorname{erf}(y)$ is the complement of the error function. Eq. (2.11) then becomes:

$$\phi_o{}^i = Z_i E_m + \sum_{j=1(\neq i)}^{N} Z_j\, U(r_i - r_j) - \int_V d^3r'\ \delta n_e(r')\, U(r_i - r'), \qquad (2.17)$$

where E_m is the Madelung energy of a simple cubic lattice with $Z = 1$ and lattice constant L. It is now only necessary to sum and integrate over particles in the unit cell. The process is most conveniently carried out by temporarily centering the unit cell on the i^{th} ion, so that any particle which is more distant than L/2 from the i^{th} ion in any of the three coordinates is replaced by its nearest image. This representation also saves computer time because values of U(r) for each mesh point can be stored in arrays at the beginning of each computation. The chemical potential at each ion can thus be computed accurately and with relative ease.

After iterating to obtain an electron distribution consistent with the TFD equation and also satisfying the boundary conditions, we integrate over the unit cell to compute the relevant thermodynamic properties. At T = 0 ^{o}K, the Helmholtz free energy per ion is:

$$F = E_e + E_x + W$$

$$= N^{-1} \{ \int_V d^3r \, \frac{3}{10}(3\pi^2)^{2/3} \, n_e^{5/3} - \int_V d^3r \, \frac{3}{4} (3/\pi)^{1/3} \, n_e^{4/3}$$

$$- \int_V d^3r \, \frac{1}{2} n_e \phi + \sum_{i=1}^{N} \frac{1}{2} Z_i \phi_o^i \}, \qquad (2.18)$$

where E_e, E_x, and W are respectively the average kinetic, exchange, and potential energies per ion. Equation (2.18) is evaluated numerically, using integration by parts in the subcells to eliminate singularities of the integrands in the vicinity of ions.

In the one-dimensional TFD problem, radial symmetry allows one to express the bulk pressure P in terms of the kinetic and exchange pressures of an electron gas at a density equal to the electron density at the surface of the atom. To obtain the pressure for the three-dimensional case, we make use of the more general expression from the virial theorem (Feynman, et al., 1949):

$$P = (2E_e + E_x + W) \; / \; 3v, \qquad (2.19)$$

where v is the average volume per ion. The energies must be computed quite accurately because some cancellation is involved in evaluating the pressure, particularly at lower pressures. Following Salpeter and

Zapolsky (1967), the correlation energy and pressure are assumed to be nonlocal quantities, to be evaluated using the average electron density and then simply added to the TFD results.

CHAPTER 3

SOLID-STATE RESULTS

Results for H-He Mixtures

The zero temperature energies and pressures were evaluated for specified values of the ion spacing parameter r_s [$=(3v/4\pi)^{1/3}$] and composition x [= number fraction of ions with higher atomic number] for each of the three lattices. The values of the ion spacing parameters were chosen to predict a pressure approximating one of our pressures of interest (10, 100, or 1000 Mbar), and were estimated from one-dimensional TFD calculations. Table 1 shows the results for H-He mixtures. The Helmholtz energies [F] and Gibbs energies [G = F + Pv] are given in atomic units per ion and have a numerical accuracy of $\sim$ a few x 10^{-4} au/ion. The tabulated data correspond to a "large" number of mesh points in the three-dimensional unit cells; i.e., extrapolated from results using 21^3 mesh points per octant of each unit cell and test runs with 41^3 mesh points.

The thermodynamic properties of simple cubic lattices with an equal number of hydrogen and helium atoms were calculated for three different ion arrangements in order to extend the range of energies of the data base. (Changing the ion positions for the bcc lattice [with 2 ions per unit cell] and the fcc lattice [with 4 ions per unit cell] merely redefines the position of the unit cell in the crystal.) These

Table 1

Zero Temperature TFD Results for H-He Mixtures

Lattice	x	r_s	P(Mbar)	F(au/ion)	G(au/ion)
bcc	0.0*	1.15225	10.0482	-0.8613	-0.6425
sc	0.0	1.15225	10.2297	-0.8554	-0.6326
bcc	0.5	1.26937	10.0656	-2.6300	-2.3370
fcc	0.5	1.26937	10.1247	-2.6279	-2.3330
sc	0.5[a]	1.26937	10.2274	-2.6229	-2.3251
sc	0.5[b]	1.26937	10.3472	-2.6190	-2.3177
sc	0.5[c]	1.26937	10.5651	-2.6128	-2.3051
bcc	1.0*	1.36814	10.0805	-4.3983	-4.0308
sc	1.0	1.36814	10.3784	-4.3850	-4.0066
bcc	0.0*	0.78019	100.248	-0.3791	+0.2987
sc	0.0	0.78019	101.190	-0.3674	+0.3169
bcc	0.5	0.86933	100.345	-1.9896	-1.0511
fcc	0.5	0.86933	100.779	-1.9841	-1.0416
sc	0.5[a]	0.86933	101.213	-1.9743	-1.0276
sc	0.5[b]	0.86933	101.898	-1.9652	-1.0121
sc	0.5[c]	0.86933	103.321	-1.9486	-0.9822
bcc	1.0*	0.94319	100.422	-3.5995	-2.3999
sc	1.0	0.94319	102.006	-3.5697	-2.3511
bcc	0.0*	0.51451	1001.35	+1.1348	+3.0765
sc	0.0	0.51451	1006.53	+1.1567	+3.1085
bcc	0.5	0.57848	1001.89	+0.0966	+2.8578
fcc	0.5	0.57848	1004.63	+0.1089	+2.8777
sc	0.5[a]	0.57848	1006.71	+0.1265	+2.9010
sc	0.5[b]	0.57848	1010.67	+0.1457	+2.9311
sc	0.5[c]	0.57848	1019.77	+0.1849	+2.9954
bcc	1.0*	0.63077	1002.29	-0.9406	+2.6406
sc	1.0	0.63077	1011.01	-0.8810	+2.7314

* Value for x=0 and x=1 are essentially the same for bcc and fcc lattices.

[a] Protons at sc lattice sites # 1, 4, 6, and 7 (see Figure 1).

[b] Protons at sc lattice sites # 1, 2, 7, and 8.

[c] Protons at sc lattice sites # 1, 3, 5, and 7.

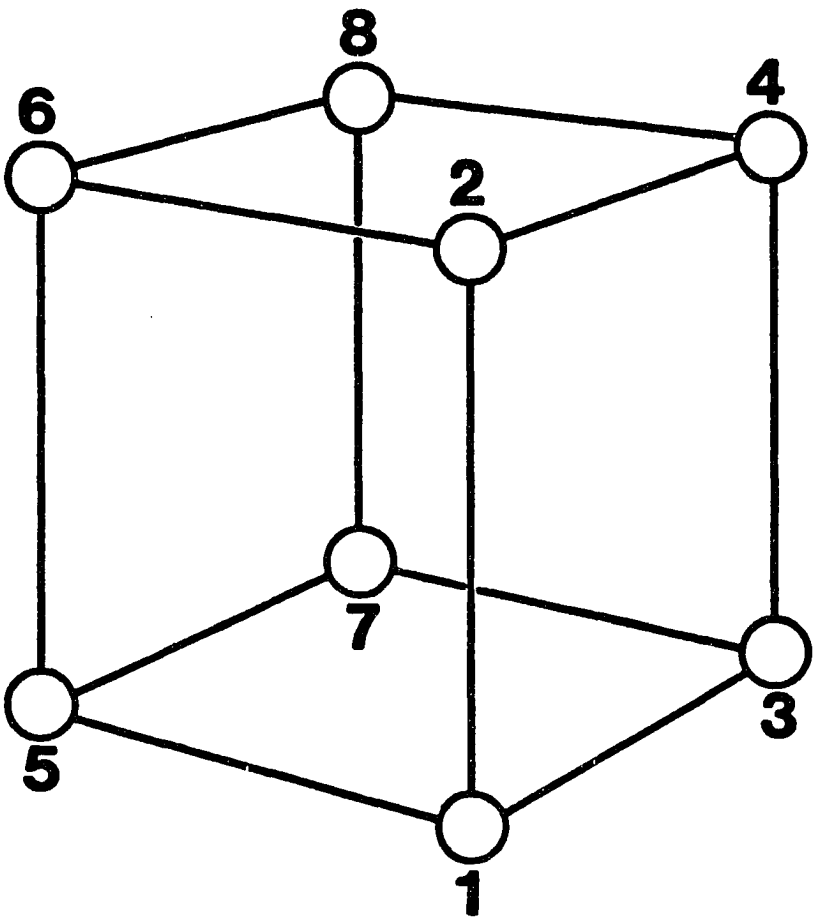

Figure 1. Ion Sites for Simple Cubic Lattices. — Simple cubic (sc) lattice ion positions corresponding to the zero temperature results in Tables 1 through 6.

different sc configurations are footnoted a, b, and c in Table 1, with the corresponding ion positions shown in Figure 1. The lattice resembling the NaCl structure [footnoted a] has the lowest total energy of the sc lattices, but still has an energy greater than the fcc or bcc lattices with an equal number of hydrogen and helium atoms. The bcc lattice was found to be the most stable of the lattices studied with this composition. These relative stabilities are also predicted by the two-component-plasma [TCP] model with an assumed uniform electron background (Dyson, 1971).

To within numerical error, the total energies for the bcc and fcc lattices are indistinguishable for the end members. That is, for pure hydrogen and pure helium, we are unable to determine the more stable lattice stucture using TFD theory. Calculations using other models do predict noticeable differences in the energies ($\sim$ 0.01 au/ion) between these two structures for helium. Free electron perturbation theory results find the zero temperature bcc lattice to have a lower energy at all pressures (Friedli and Ashcroft, 1975). But calculations using linear-muffin-tin orbital theory (Young, et al., 1981) indicate that the fcc lattice should be the more stable configuration in the 10 to 1000 Mbar pressure range.

The zero temperature equations of state for pure hydrogen and pure helium constructed from the three-dimensional TFD results are shown in Figure 2 [labelled TFD]. The TFD pressures are from the bcc lattice results and are just slightly higher ($\lesssim$ 0.1%) that for the one-dimensional case. For comparison, we show for pure helium the

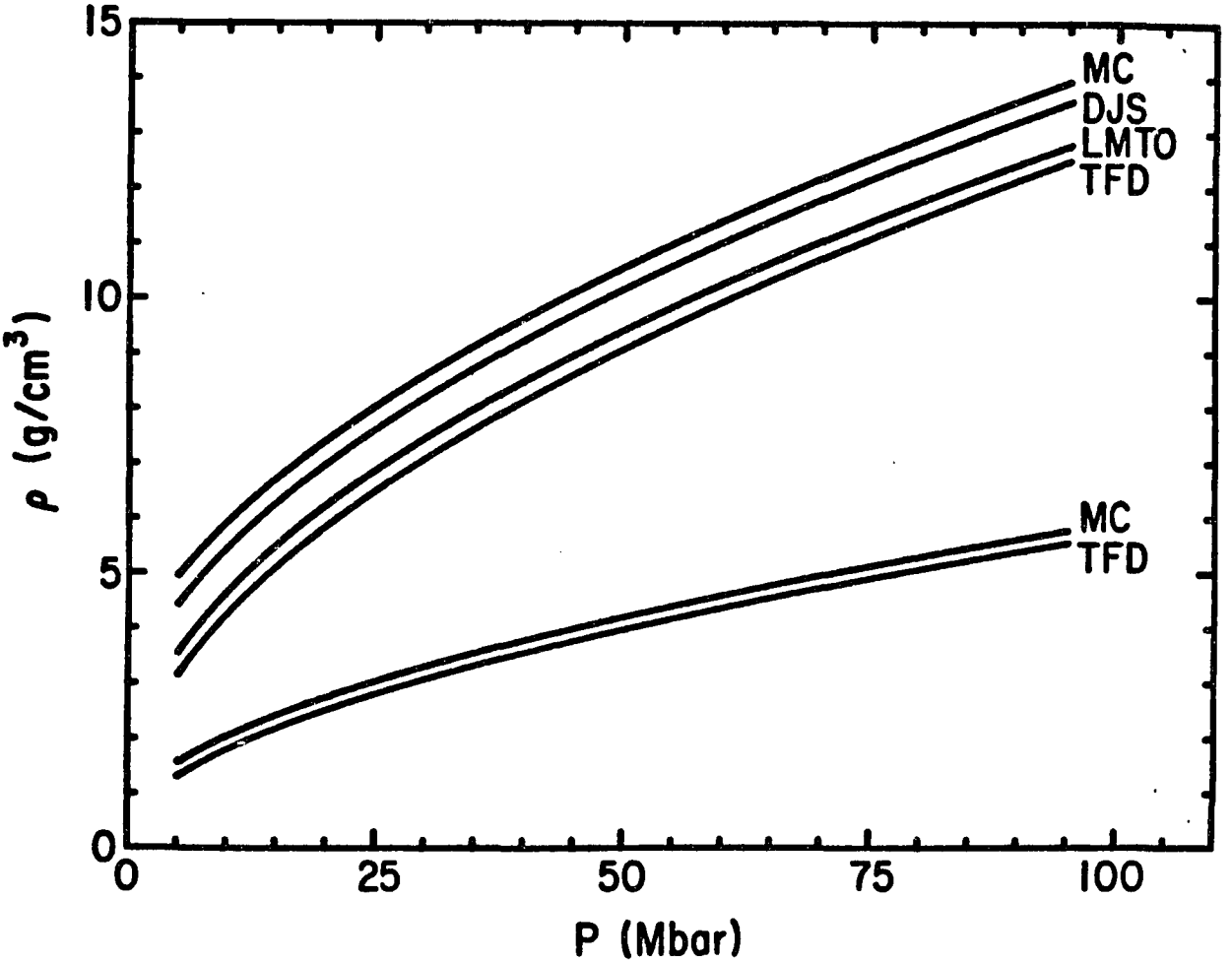

Figure 2. Equations of State for Hydrogen and Helium. — Zero temperature pressure-density relations for He (upper four curves) and H (lower two curves). MC, computed using the linear screening theory of Hubbard (1972); DJS, computed using a similar theory for He, but carried to one higher order in the perturbation expansion; LMTO, from the crystal-state calculations of Young, et al.; TFD, computed for bcc lattices using TFD theory.

pressure-density curves from Hubbard (1972) [MC], Stevenson (1975) [DJS], and Young, et al. (1981) [LMTO]. Also shown is the pure hydrogen curve from Hubbard (1972) [MC]. Hubbard's results were obtained from Monte Carlo studies assuming a fully ionized mixture with simple screening. Stevenson also assumed a fully ionized mixture with screening, but carried out the perturbation expansion to second order. The results of Young, et al. were derived using linear-muffin-tin-orbital theory. All curves are standardized to include the correlation pressure and to be at zero pressure.

It is seen that the various theories produce little difference in the pressure-density curve for pure hydrogen, while for pure helium somewhat larger differences exist. As expected, both model assuming fully ionized helium with screening agree relatively well with each other, with the Monte Carlo curve being quite similar to the equation of state of a helium atom without screening. On the other hand, the TFD and LMTO models, which are independent theories, predict somewhat higher pressures for helium. This is expected because the lower energies produced by the tighter binding of the electrons to the ions. Treatment of the electron distribution as a perturbation from a uniform electron distribution may be of questionable validity for helium at pressures near or below its metallization pressure ($\sim 10^2$ Mbar). At such low pressures, the TFD and LMTO models might produce more accurate electron distributions away from the ions and a better equation of state for helium.

The free energies and densities for mixtures are often calculated assuming ideal mixing. However, the non-ideality of a mixture plays an essential role in determining the instability of a mixture to phase separation. The deviation from ideal mixing of a thermodynamic parameter A is given by:

$$\delta A(x,P) = A(x,P) - [(1-x)\,A(0,P) + x\,A(1,P)], \qquad (3.1)$$

where again x is the composition parameter. Values of δG and $\delta V/V$ for the H-He mixtures are computed from our TFD results for each of the pressure groups and are shown in Table 2. Note that the deviations from ideal mixing for the H-He solutions are quite small [$\lesssim 10^{-2}$ au/ion].

We can compare the zero temperature TFD results with those computed for a two-component-plasma [TCP] with a uniform electron background and a two-component system with simple screening. For a mixture of ions with charges Z_1 and Z_2, assuming simple screening, the Helmholtz energy per ion at T = 0 ^{o}K is given by (Hubbard and Slattery, 1971):

$$F = \langle Z\rangle\,[1.105\,s^{-2} - 0.458\,s^{-1}] + \frac{1}{2}\langle Z^2\rangle\,\psi_o + \frac{1}{2N}\sum_{i=1}^{N}\sum_{(i\neq j)}^{N} Z_i Z_j\,\psi(r_i - r_j), \qquad (3.2)$$

where $\langle Z^2\rangle = (1-x)\,Z_1^2 + x\,Z_2^2$, s is the electron spacing parameter [$s=(3V/4\pi N\langle Z\rangle)^{1/3}$], the electron correlation energy is neglected, and ψ and ψ_o are functions defined by Hubbard and Slattery, which depend

Table 2

Mixing Properties for H-He Solutions with x = 0.5

	Lattice	r_s	δG(au/ion)	δV/V
P = 10 Mbar:	bcc	1.27067	-0.0002	-0.0001
	fcc	1.27183	+0.0019	+0.0026
	sc[a]	1.27386	-0.0027	-0.0045
	sc[b]	1.27622	+0.0012	+0.0011
	sc[c]	1.28053	+0.0074	+0.0112
P = 100 Mbar:	bcc	0.86984	-0.0003	-0.0001
	fcc	0.87048	+0.0051	+0.0021
	sc[a]	0.87112	-0.0058	-0.0026
	sc[b]	0.87213	+0.0033	+0.0009
	sc[c]	0.87422	+0.0199	+0.0081
P = 1000 Mbar:	bcc	0.57868	-0.0005	-0.0001
	fcc	0.57896	+0.0118	+0.0014
	sc[a]	0.57917	-0.0114	-0.0015
	sc[b]	0.57959	+0.0078	+0.0006
	sc[c]	0.58053	+0.0470	+0.0055

[a] Protons at sc lattice sites # 1, 4, 6, and 7 (see Figure 1).
[b] Protons at sc lattice sites # 1, 2, 7, and 8.
[c] Protons at sc lattice sites # 1, 3, 5, and 7.

on the Ewald potential U(r), the Madelung energy for a simple cubic lattice with Z = 1 and lattice constant L, and the Lindhard dielectric function ε_k. For the TCP model, the free energy is given by equation (3.2) with $\varepsilon_k = 1$. The energy and density for a specified pressure and composition are found by iterating to get the correct value of s.

The Gibbs energies of mixing for the bcc and fcc lattices have been computed for both the screened and unscreened cases and compared with the TFD values. Figures 3 and 4 show the excess Gibbs energies as a function of pressure for the bcc and fcc lattices, respectively. For the bcc case, δG has been computed for pressures up to 10^6 Mbar to test for convergence, which should occur because the electron distribution becomes uniform for all three models in the high pressure limit. In Figure 3, we see that the three curves are converging, although at a rather slow rate. Note that for each lattice, the TFD mixing energies are at all pressures $\sim$ 0.01 - 0.02 au/ion (or 3000 to 6000 ^{o}K) lower than those derived using the linear screening model.

It is clear that the predicted stability of hydrogen-helium mixtures depends strongly on the manner in which the electrons are allowed to respond to the ion potentials. The Gibbs mixing energies are not a simple function of the electron densities near the "surfaces" of the atoms. This is evident from the fact that the bcc values of δG for the simple screening model are greater than those for a two-component-plasma without screening, while the δG values for the TFD model are significantly smaller than for the TCP case. The "surface" electron densities for the TFD model are lower those of both

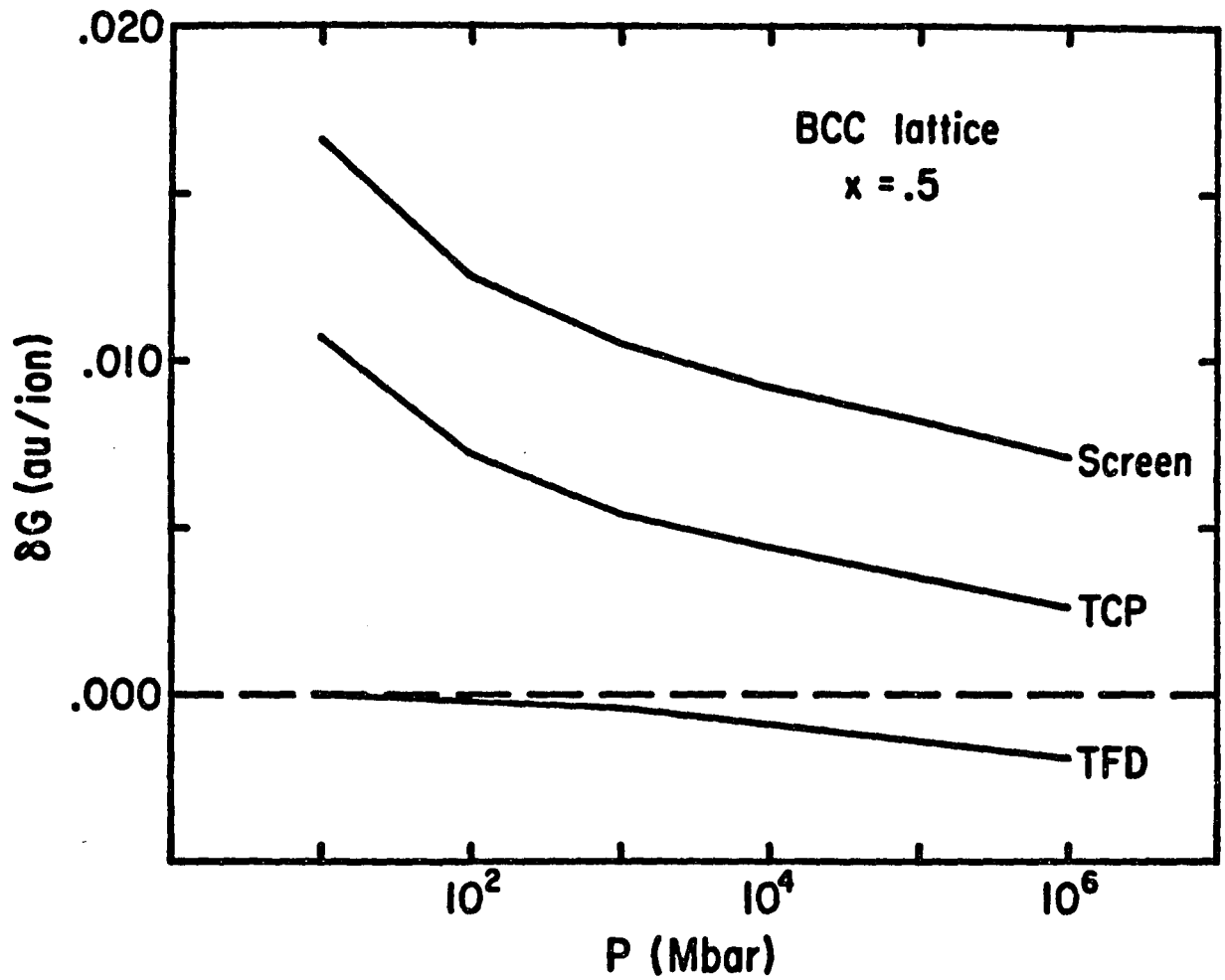

Figure 3. Excess Gibbs Energies for H-He BCC Lattices. — Gibbs energies of mixing for a bcc lattice of hydrogen and helium, with a proton located at 0, 0, 0, and a helium nucleus located at L/2, L/2, L/2. Screen, calculated using linear response theory; TCP, calculated assuming a uniform electron background; TFD, three-dimensional TFD results.

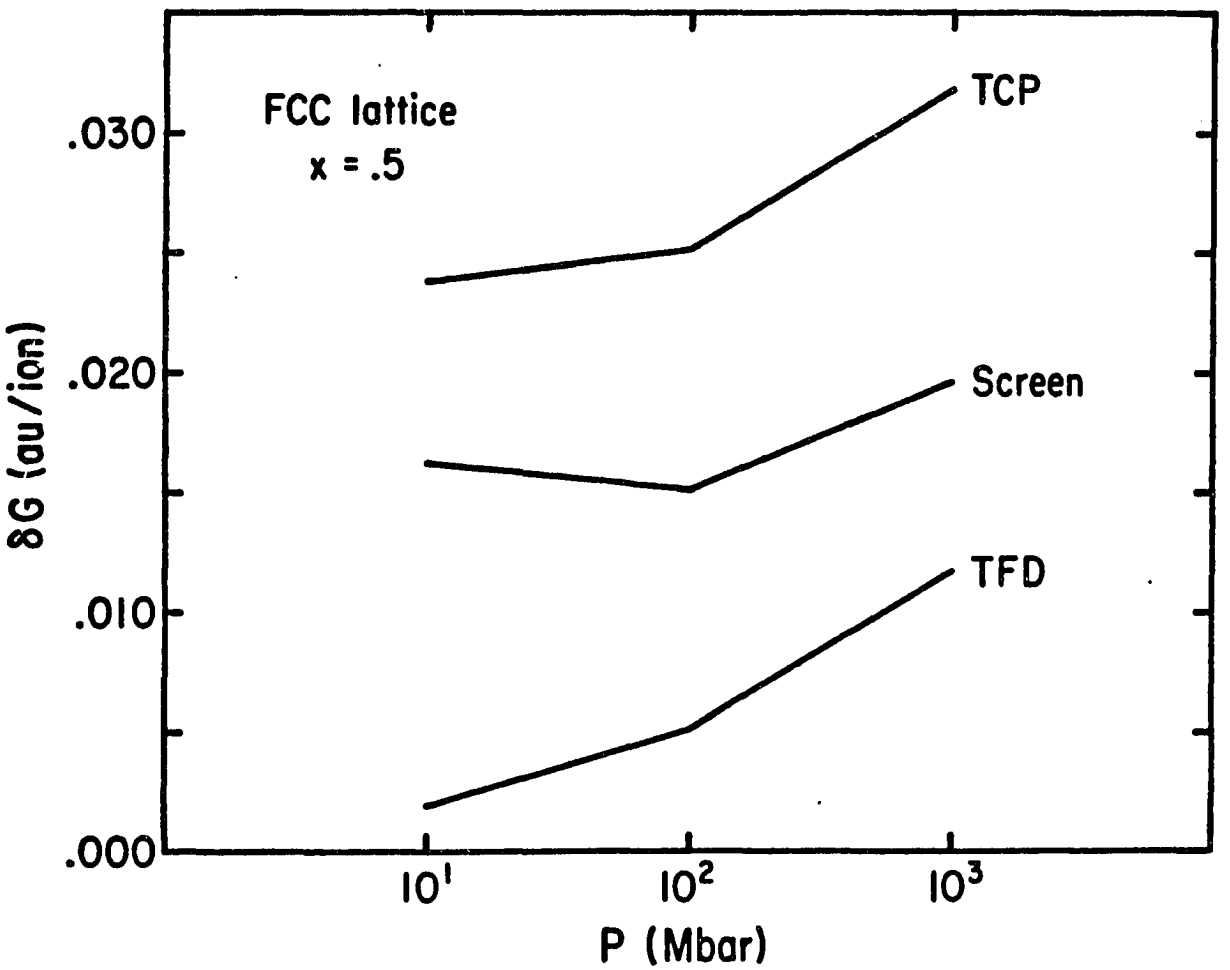

Figure 4. Excess Gibbs Energies for H-He FCC Lattices. — Gibbs energies of mixing for an fcc lattice of hydrogen and helium, with protons located at 0, 0, 0, and L/2, 0, L/2, and helium nuclei located at 0, L/2, L/2, and L/2, L/2, 0. Nomenclature is the same as in Figure 3.

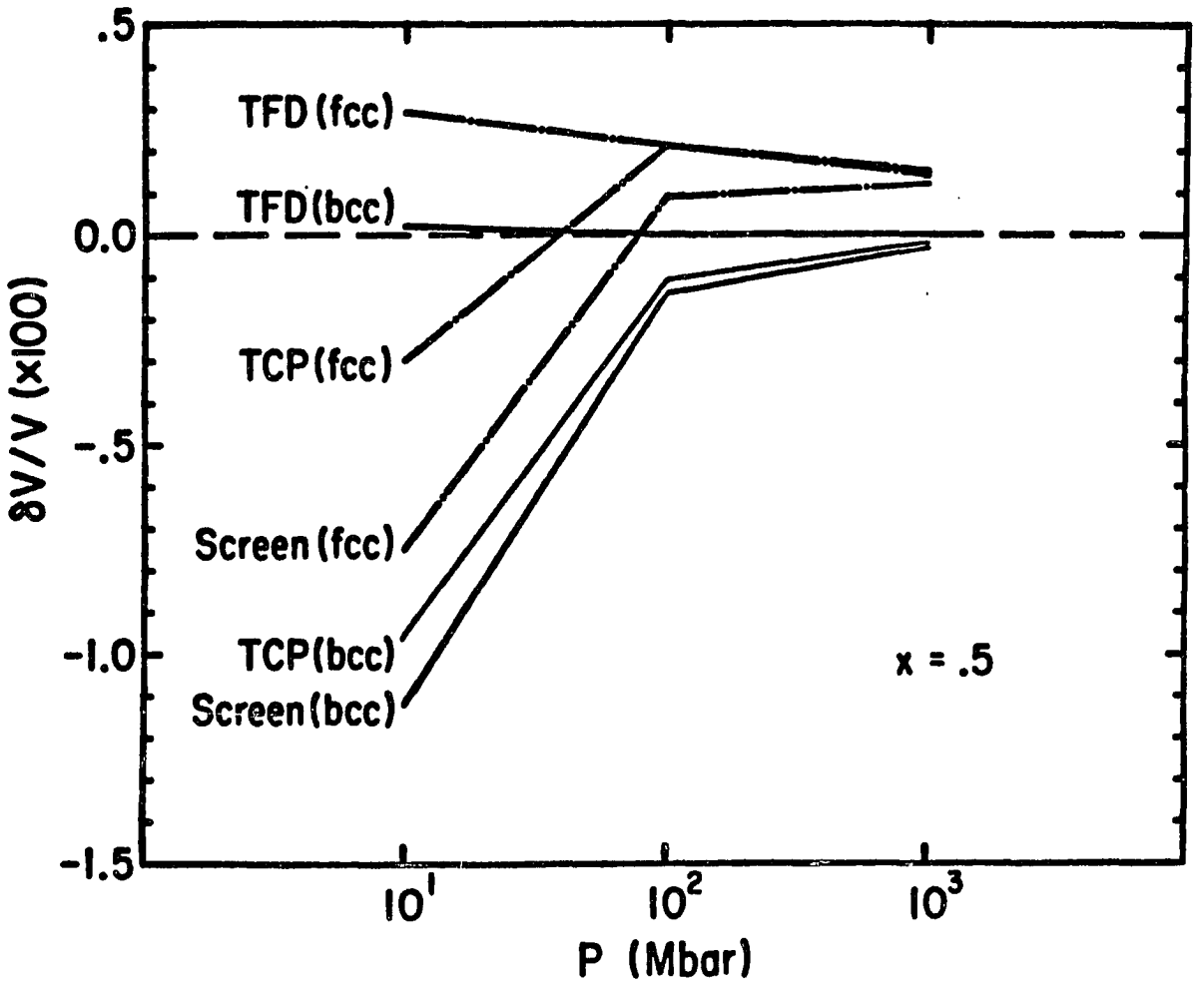

Figure 5. Excess Volumes for H-He Lattices. — Excess volumes of mixing in percent as a function of pressure, for an equal number of hydrogen and helium ions in various lattices. Stevenson's (1975) results are off scale and range from about -6% at 10 Mbar to about -3% at 100 Mbar.

the linear response model and the unscreened plasma, which of course has the highest "surface" electron density. However, linear response theory calculations for hydrogen in the sc configuration indicate that the electron densities along a path between a proton and one of its nearest neighbors are everywhere greater than the average electron density. This is a clear example of just how weak the electrons respond to the electrostatic potential in the perturbation model, and this may be the reason the linear response mixing energies for the bcc lattices are greater than those for the TCP model.

Finally, Figure 5 shows the excess volumes of mixing as a function of pressure for the various theories. The "additive volume law" corresponds to $\delta V/V = 0$ for all compositions. Deviations from the additive volume las are rather small for all models ($\lesssim$ 1%), and go to zero in the high pressure limit. Our TFD results predict that the mixing volumes should be $\lesssim$ 0.1% of the total volume. Even lattices assuming a uniform electron background or simple screening do not approach Stevenson's values of $\delta V/V \sim -6\%$ at 10 Mbar.

Results for H-C and H-O Mixtures

Similar sets of calculations were carried out for both hydrogen-carbon and hydrogen-oxygen mixtures. Tables 3 and 4 show the results for the H-C and H-O systems, respectively. (The results for pure hydrogen can be found in Table 1.) The calculations were performed for the same lattice configurations as those used for the H-He calculations, and the values of r_s were again chosen to predict

Table 3

Zero Temperature TFD Results for H-C Mixtures*

Lattice	x	r_s	P(Mbar)	F(au/ion)	G(au/ion)
bcc	0.5	1.49356	10.164	-27.659	-27.177
fcc	0.5	1.49356	10.628	-27.640	-27.136
sc	0.5[a]	1.49356	9.804	-27.678	-27.213
sc	0.5[b]	1.49356	10.862	-27.631	-27.116
sc	0.5[c]	1.49356	12.504	-27.567	-26.974
bcc	1.0	1.72508	10.164	-54.458	-53.714
fcc	1.0	1.72508	10.161	-54.458	-53.714
sc	1.0	1.72508	10.758	-54.417	-53.631
bcc	0.5	1.05228	101.07	-26.634	-24.957
fcc	0.5	1.05228	104.35	-26.575	-24.844
sc	0.5[a]	1.05228	99.80	-26.657	-25.001
sc	0.5[b]	1.05228	105.82	-26.542	-24.787
sc	0.5[c]	1.05228	116.69	-26.358	-24.422
bcc	1.0	1.22881	100.92	-52.896	-50.230
fcc	1.0	1.22881	100.91	-52.896	-50.231
sc	1.0	1.22881	104.35	-52.788	-50.032
bcc	0.5	0.71871	1006.8	-22.976	-17.654
fcc	0.5	0.71871	1028.6	-22.821	-17.384
sc	0.5[a]	0.71871	1001.2	-23.010	-17.718
sc	0.5[b]	0.71871	1036.4	-22.745	-17.267
sc	0.5[c]	0.71871	1108.4	-22.263	-16.404
bcc	1.0	0.84637	1005.3	-47.113	-38.437
fcc	1.0	0.84637	1005.2	-47.114	-38.438
sc	1.0	0.84637	1025.0	-46.862	-38.015

* Values for pure H (x = 0) can be found in Table 1.

[a] Protons at sc lattice sites # 1, 4, 6, and 7 (see Figure 1).
[b] Protons at sc lattice sites # 1, 2, 7, and 8.
[c] Protons at sc lattice sites # 1, 3, 5, and 7.

Table 4

Zero Temperature TFD Results for H-O Mixtures*

Lattice	x	r_s	P(Mbar)	F(au/ion)	G(au/ion)
bcc	0.5	1.55601	10.221	-53.070	-52.522
fcc	0.5	1.55601	10.839	-53.043	-52.462
sc	0.5[a]	1.55601	9.461	-53.114	-52.607
sc	0.5[b]	1.55601	11.008	-53.041	-52.450
sc	0.5[c]	1.55601	13.298	-52.944	-52.231
bcc	1.0	1.81762	10.193	-105.282	-104.411
fcc	1.0	1.81762	10.187	-105.283	-104.412
sc	1.0	1.81762	10.888	-105.230	-104.299
bcc	0.5	1.10554	101.53	-51.915	-49.962
fcc	0.5	1.10554	106.01	-51.828	-49.789
sc	0.5[a]	1.10554	98.76	-51.978	-50.078
sc	0.5[b]	1.10554	107.46	-51.796	-49.728
sc	0.5[c]	1.10554	122.48	-51.516	-49.160
bcc	1.0	1.30600	101.11	-103.469	-100.262
fcc	1.0	1.30600	101.09	-103.470	-100.264
sc	1.0	1.30600	105.22	-103.326	-99.989
bcc	0.5	0.76153	1010.1	-47.687	-41.336
fcc	0.5	0.76153	1040.4	-47.445	-40.904
sc	0.5[a]	0.76153	997.9	-47.785	-41.510
sc	0.5[b]	0.76153	1048.7	-47.357	-40.763
sc	0.5[c]	0.76153	1148.8	-46.606	-39.382
bcc	1.0	0.90737	1006.3	-96.568	-85.864
fcc	1.0	0.90737	1006.4	-96.570	-85.867
sc	1.0	0.90737	1030.6	-96.218	-85.257

* Values for pure H (x = 0) can be found in Table 1.

[a] Protons at sc lattice sites # 1, 4, 6, and 7 (see Figure 1).
[b] Protons at sc lattice sites # 1, 2, 7, and 8.
[c] Protons at sc lattice sites # 1, 3, 5, and 7.

pressures close to 10, 100, or 1000 Mbars. Because of the greater charge of the second atomic species, the numerical error in the H-C and H-O results is somewhat larger, with the Helmholtz and Gibbs energies being accurate to $\sim 1 \times 10^{-3}$ au/ion.

In Tables 3 and 4, it is seen that the total energies for the bcc and fcc lattices are essentially the same for pure carbon and oxygen, although there is some suggestion that the fcc lattice is slightly more stable. This differs from the TCP model (with a uniform electron background), where for pure systems, the bcc energies are always slightly lower than the fcc energies (Brush, et al., 1966).

For structures with a composition of $x = 0.5$, it is interesting to note that the sc lattice resembling the NaCl structure is the most stable configuration for both H-C and H-O mixtures. This is also the case for the TCP model (Dyson, 1971), where the NaCl configuration is found to be more stable than the bcc (or CsCl) configuration provided $Z_2/Z_1 \geq 5$.

The mixing properties for the H-C and H-O solutions have been evaluated and are listed in Tables 5 and 6, respectively. Although the mixing energies [δG] are relatively small ($\lesssim 1\%$ of the total energies), the values of δG for the H-C and H-O mixtures are roughly 10 to 20 times larger (in absolute value) than those for the H-He mixtures. Also, the deviations from the "additive volume law" are somewhat larger, with typical values of $\delta V/V$ being $\sim$ a few per cent. Larger deviations from ideal mixing are of course expected for mixtures of elements with larger charge differences.

Table 5

Mixing Properties for H-C Solutions with x = 0.5

	Lattice	r_s	$\delta V/V$	δG(au/ion)	δG_{TCP}(au/ion)
P = 10 Mbar:	bcc	1.49710	+0.0013	+0.001	+0.372
	fcc	1.50710	+0.0211	+0.019	+0.730
	sc[a]	1.48934	-0.0359	-0.042	+0.059
	sc[b]	1.51214	+0.0102	+0.005	+0.550
	sc[c]	1.54752	+0.0766	+0.069	+1.782
P = 100 Mbar:	bcc	1.05408	+0.0014	+0.004	+0.271
	fcc	1.05957	+0.0169	+0.063	+0.682
	sc[a]	1.05195	-0.0185	-0.079	-0.081
	sc[b]	1.06203	+0.0103	+0.035	+0.482
	sc[c]	1.08025	+0.0595	+0.220	+1.928
P = 1000 Mbar:	bcc	0.71955	+0.0012	+0.014	+0.220
	fcc	0.72223	+0.0123	+0.169	+0.770
	sc[a]	0.71886	-0.0104	-0.158	-0.242
	sc[b]	0.72319	+0.0077	+0.107	+0.511
	sc[c]	0.73206	+0.0432	+0.590	+2.472

[a] Protons at sc lattice sites # 1, 4, 6, and 7 (see Figure 1).
[b] Protons at sc lattice sites # 1, 2, 7, and 8.
[c] Protons at sc lattice sites # 1, 3, 5, and 7.

Table 6

Mixing Properties for H-O Solutions with x = 0.5

	Lattice	r_s	δV/V	δG(au/ion)	δG_{TCP}(au/ion)
P = 10 Mbar:	bcc	1.56070	+0.0023	+0.002	+0.751
	fcc	1.57380	+0.0272	+0.029	+1.507
	sc[a]	1.54458	-0.0544	-0.072	+0.091
	sc[b]	1.57739	+0.0100	+0.002	+1.130
	sc[c]	1.62596	+0.0961	+0.099	+3.704
P = 100 Mbar:	bcc	1.10802	+0.0023	+0.009	+0.583
	fcc	1.11527	+0.0217	+0.097	+1.405
	sc[a]	1.10353	-0.0264	-0.131	-0.125
	sc[b]	1.11762	+0.0119	+0.051	+1.004
	sc[c]	1.14194	+0.0738	+0.331	+3.859
P = 1000 Mbar:	bcc	0.76270	+0.0019	+0.030	+0.471
	fcc	0.76622	+0.0155	+0.273	+1.515
	sc[a]	0.76128	-0.0144	-0.254	-0.409
	sc[b]	0.76719	+0.0089	+0.174	+1.022
	sc[c]	0.77883	+0.0527	+0.925	+4.719

[a] Protons at sc lattice sites # 1, 4, 6, and 7 (see Figure 1).
[b] Protons at sc lattice sites # 1, 2, 7, and 8.
[c] Protons at sc lattice sites # 1, 3, 5, and 7.

Also shown in Tables 5 and 6 are the Gibbs mixing energies for the two-component-plasma model [δG_{TCP}]. The values for δG_{TCP} were found using eq. (3.2) and correspond to the pressures indicated in the left columns of the tables. The TCP mixing energies are generally found to be greater than the TFD values, with typical differences in δG between the two models being ~ 1 au/ion. If, in the liquid phase, the TFD mixing energies are lower than the TCP mixing energies by similar amounts, the TFD phase separation temperatures should be expected to be ~ 1 au (or $\sim 10^5$ ^{o}K) lower than the TCP temperatures. This will be discussed further in Chapter 6.

CHAPTER 4

MODEL POTENTIALS

In order to assess the mixing properties of fluid mixtures, it is necessary to first find an effective potential (or pseudopotential) which will fit all of the solid-state data. In addition to predicting the total energy and pressure of each data point, the potential must also be able to reproduce the mixing properties of each system. It is essential that the pseudopotential adequately predicts the small deviations from ideal mixing in the energy for each lattice.

The form of the pseudopotential we have chosen is similar to the potential of a two-component-plasma [TCP] without screening (i.e., with a uniform electron background). This is prompted by the fact that the total energies of bcc and fcc lattices for pure (one-component) TCP systems with no screening differ by less than 0.01% (Brush, et al., 1966), and therefore should readily fit the TFD data. But because the TFD model allows the electron clouds to be tightly bound to the nuclei, the effective ion charges seen by the electron gas away from the nuclei will be smaller than in the TCP case. This suggests that the pseudopotential should have a form similar to that of the TCP potential, but with smaller effective ion charges, which in general will be a function of the pressure.

For a two-component system with effective charges Z_1^* and Z_2^*, an average charge of $\langle Z^* \rangle = (1-x)\, Z_1^* + x\, Z_2^*$, and an electron spacing parameter s [$= r_s/\langle Z^* \rangle^{1/3}$], the model Helmholtz energy takes the form:

$$F = E_e + E_x + W + E_{si} , \qquad (4.1)$$

where E_e is the zero temperature electron kinetic energy, E_x is the first-order exchange energy between electrons, W is the Coulomb energy, and E_{si} is an additional structure-independent energy, which is found by fitting to the TFD data. The first two terms on the RHS are given by:

$$E_e + E_x = \langle Z^* \rangle \, [1.105\ s^{-2} - 0.458\ s^{-1}] \text{ au/ion}, \qquad (4.2)$$

where again $\langle Z^* \rangle$ is the average <u>effective</u> charge. The Coulomb (or Madelung) energy for a multi-component lattice is (Hubbard, 1972):

$$W = 0.5 \langle (Z^*)^2 \rangle \, E_m + N^{-1} \sum_{i<j}^{N} Z_i^* Z_j^* U(r_j - r_i) , \qquad (4.3)$$

where N is the number of ions per unit cell, $\langle (Z^*)^2 \rangle = (1-x)\,(Z_1^*)^2 + x\,(Z_2^*)^2$, E_m is the Madelung energy of a simple cubic lattice with Z=1 and unit cell volume Nv, and U(r) is the Ewald potential discussed in Chapter 2. The values of Z_1^* and Z_2^* are also found by fitting to the TFD data.

The effective ion charges will in general be a function of the pressure, but in practice must be fitted to a function of the ion spacing parameters because the pressure is not a pre-determined

quantity. The form for the effective ion charges we have chosen is:

$$Z_i^*(r_{s,i}) = Z_i \exp[-\alpha_i r_{s,i} - \beta_i r_{s,i}^2] , \qquad (4.4)$$

where Z_i and $r_{s,i}$ are the actual charge and the ion spacing parameter of the i^{th} ion, and α_i and β_i are constants determined from the fitting procedure and are listed in Tables 7, 8, and 9 for the H-He, H-C, and H-O mixtures, respectively. Note that in the high pressure limit ($r_s \to 0$), the effective ion charges will correctly approach the actual charge of their respective ions. For a mixture of composition x and ion spacing parameter r_s, the values for $r_{s,1}$ and $r_{s,2}$ are found by simultaneously solving:

$$(1-x)\, r_{s,1}^3 + x\, r_{s,2}^3 = r_s^3 \qquad (4.5)$$

and

$$P_1(r_{s,1}) = P_2(r_{s,2}) , \qquad (4.6)$$

where P_1 and P_2 represent the T=0 ^oK pressures for the end members, which are estimated from one-dimensional TFD calculations. Eq. (4.5) is the "additive volume law" and is sufficient to use here because the volumetric deviations from ideal mixing are small.

The structure-independent term for the pseudopotential can be separated into two parts: the first obeying ideal mixing laws, and the second representing the small non-ideal contribution. This can be written as:

$$E_{si} = (1-x)\, E_{si,1} + x\, E_{si,2} + \delta E_{si} , \qquad (4.7)$$

where the first two terms on the RHS are the contributions from the

Table 7

Constants for H-He Pseudopotentials

Eq. (4.4):	Ion	α_i	β_i
	H	0.2411	0.1287
	He	0.4037	0.0520

Eq. (4.8)	Ion	a_i	b_i	c_i	d_i
	H	1.219	0.604	0.732	0.658
	He	4.746	0.699	1.235	0.787

Eq. (4.9)	A_1	A_2
	-0.0092	0.0108

Table 8

Constants for H-C Pseudopotentials

Eq. (4.4):

Ion	α_i	β_i
H	0.2411	0.1287
C	0.6575	-0.0166

Eq. (4.8):

Ion	a_i	b_i	c_i	d_i
H	1.219	0.604	0.732	0.658
C	54.917	0.671	1.934	0.751

Eq. (4.9):

A_1	A_2
-0.125	0.110

Table 9

Constants for H-O Pseudopotentials

Eq. (4.4):

Ion	α_i	β_i
H	0.2411	0.1287
O	0.7308	-0.0341

Eq. (4.8):

Ion	a_i	b_i	c_i	d_i
H	1.219	0.604	0.732	0.658
O	105.735	0.661	2.133	0.733

Eq. (4.9):

A_1	A_2
-0.207	0.162

end members, and δE_{si} is the "excess" structure-independent energy. The form for the end members was chosen to be:

$$E_{si,i} = -a_i \left[1 - (r_{s,i})^{-b_i} \exp(-c_i (r_{s,i})^{d_i})\right] \quad \text{au/ion}, \qquad (4.8)$$

where a_i, b_i, c_i, and d_i are constants determined by fitting to both the energy and pressure of each data group, and listed in Tables 7 through 9. In the high pressure limit, E_{si} is unbounded, increasing as r_s^{-b}. But because $b < 1$, the electron kinetic energy term [$E_e \sim r_s^{-2}$] still dominates, and our model free energy correctly approaches the TCP result.

The "excess" structure-independent energy was evaluated for each of the pressure groups and fitted to a function of $r_{s,1}$:

$$\delta E_{si} = x(1-x) \left[A_1 + A_2/r_{s,1}\right] \quad \text{au/ion}, \qquad (4.9)$$

where A_1 and A_2 are constants and are also listed in Tables 7 through 9. The values of δE_{si} are small relative to typical values for the overall mixing energies, and deviations from its assumed parabolic form would have a negligible effect on our results.

Substituting the expressions for Z_1^*, Z_2^*, and E_{si} in eqs. (4.1) and (4.3), the total energies, pressures, and mixing energies are reproduced quite well. Errors for the total energies and pressure are very small, with typical residuals $\sim$ 0.1 %. In Figures 6, 7, and 8, the Gibbs mixing energies ($\delta G = G(x,P) - [(1-x)G(0,P) + xG(1,P)]$) are plotted for the H-He, H-C, and H-O mixtures, respectively, as a function of pressure for the 5 crystal structures examined with

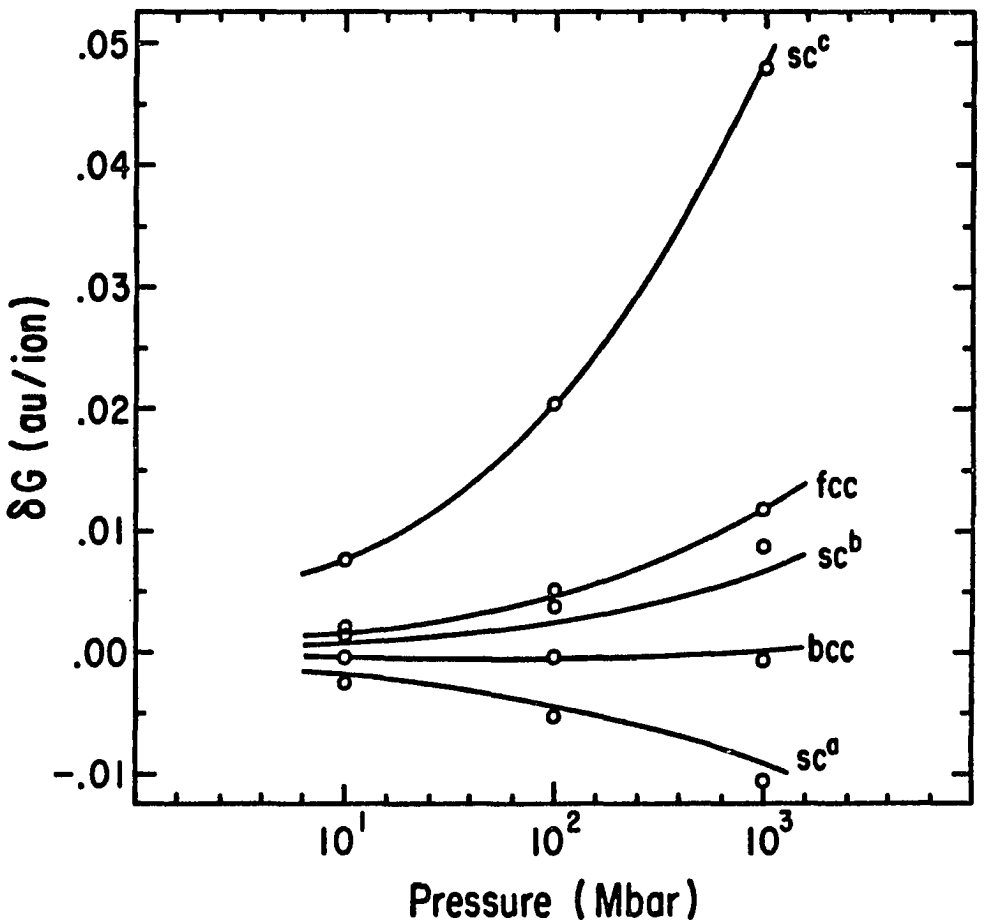

Figure 6. Gibbs Mixing Energies from H-He Pseudopotentials. -- Gibbs energies of mixing for T = 0 °K bcc, fcc, and sc lattices with H-He compositons of x = 0.5. Solid curves are determined using the pseudopotentials in Chapter 4; open circles are the solid-state data points. Footnotes for the sc lattices correspond to those in Table 1.

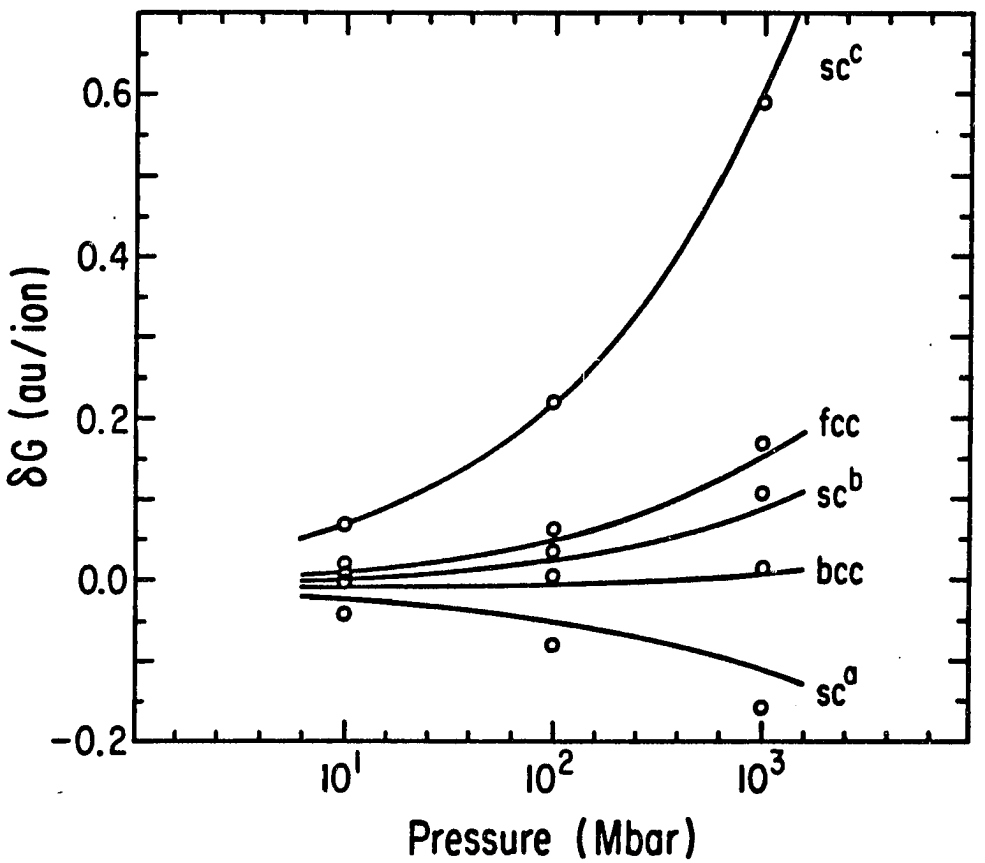

Figure 7. Gibbs Mixing Energies from H-C Pseudopotentials. — Gibbs energies of mixing for T = 0 °K bcc, fcc, and sc lattices with H-C compositions of x = 0.5. Nomenclature is the same as in Figure 6.

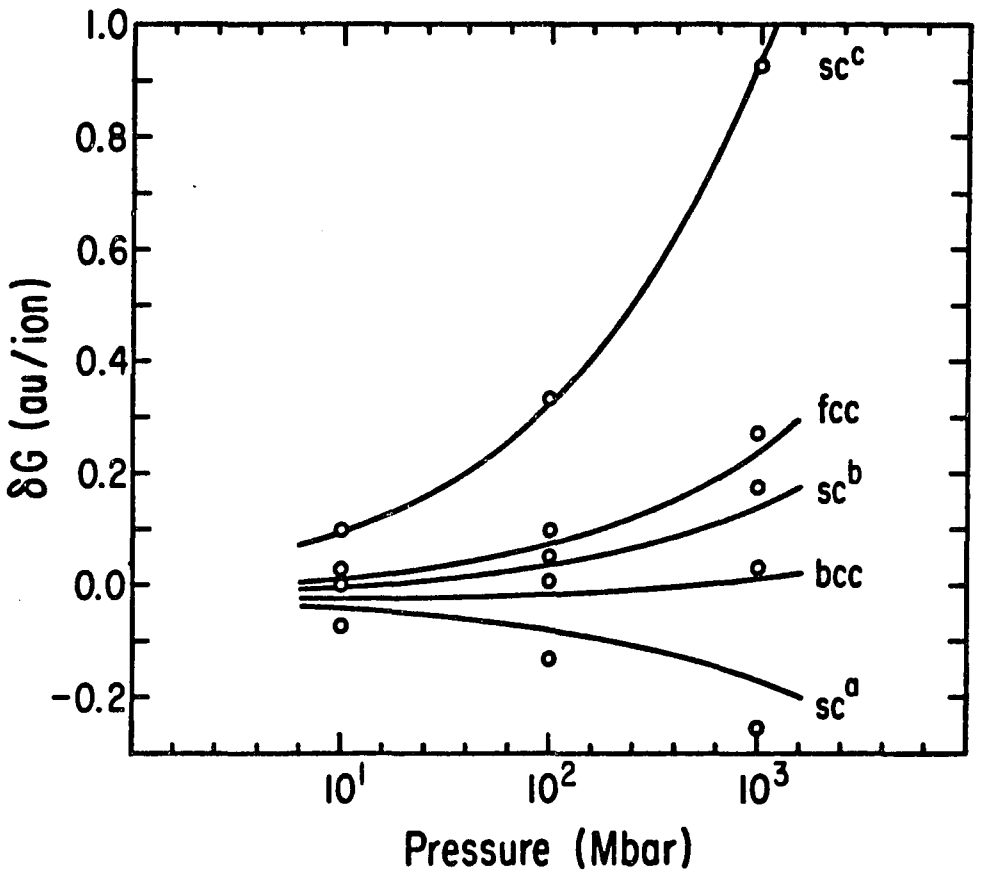

Figure 8. Gibbs Mixing Energies from H-O Pseudopotentials. — Gibbs energies of mixing for T = 0 °K bcc, fcc, and sc lattices with H-O compositions of x = 0.5. Nomenclature is the same as in Figure 6.

$x = 0.5$. The footnotes for the sc lattices correspond to those in Tables 1 through 6, and the circles are the mixing energies from the solid-state calculations. Note that there is good agreement between the zero temperature data and the pseudopotential curves.

We now have model potentials which accurately reproduces the relevant thermodynamic properties from our solid-state TFD calculations, as well as can conveniently be used in liquid-state calculations.

CHAPTER 5

LIQUID-STATE FORMALISM

Using the pseudopotentials described in Chapter 4, the equilibrium properties of fluid mixtures can be readily calculated using hard-sphere perturbation theory. This method utilizes a variational approach to assessing the properties of fluids, minimizing the free energy of the system by varying the hard-sphere diameters, and using the hard-sphere system as a reference. This approach has been developed by Mansoori and Canfield (1969) and extended to two component systems by Mansoori, et al. (1971). It has been applied to the study of two-component-plasmas by Ross and Seale (1974) for ions in a uniform negatively charged background, and by Stevenson (1975) who in addition included screening effects for the H-He system. Calculations using hard-sphere perturbation theory predict results which are quite similar to those found using Monte Carlo and molecular dynamics computations, and have the advantage of requiring relatively little computer time.

We begin by formulating the free energy of a two-component fluid based on the pseudopotentials described in Chapter 4. We assume a mixture of ions with effective charges Z_1^* and Z_2^*, immersed in a negatively charged background with a constant density of $\langle Z^* \rangle / v$. The ions are assumed to interact like hard-spheres. The Helmholtz free

energy then is given by:

$$F = F_e + E_{si} + F_{hs} + W + F_{qm} , \tag{5.1}$$

where F_e is the free energy of a uniform electron gas, E_{si} is the additional structure-independent energy described in Chapter 4, F_{hs} is the free energy for a mixture of interacting hard-spheres, W is the Coulomb energy, and F_{qm} is the high-temperature quantum mechanical correction for the hard-sphere system. The last three terms on the RHS are all structure-dependent (i.e., depend on the pair-distribution function), and therefore are a function of the hard-sphere diameters.

The free energy for a uniform electron gas is:

$$F_e = E_e + E_x + E_{corr} + F_{th} , \tag{5.2}$$

where E_e and E_x are the kinetic and exchange energies given by eq. (4.2), and E_{corr} is the electron correlation energy. For E_{corr}, we used the interpolation formula of Salpeter and Zapolsky (1967), with $\langle Z^* \rangle$ representing the charge dependence. The final term in eq. (5.2) is the first-order thermal contribution to the electron gas free energy (Landau and Lifshitz, 1969):

$$F_{th} = -\frac{1}{2}\left[\frac{4\pi}{9}\right]^{2/3} \langle Z^* \rangle s^2 T^2 \quad \text{au/ion} , \tag{5.3}$$

where T is the temperature in atomic units (1 au = 3.158 x 105 oK). Because the temperatures we are considering are much lower than the electron degeneracy temperatures, the thermal contributions to F_e are small and higher-order corrections are unimportant.

The expression for E_{si} can be found in eqs. (4.7) through (4.9). Because this term represents a fit to the zero temperature

data, no information is available on the thermal dependence this term may have. Consequently, this may affect our results for the thermal derivatives of the free energy (e.g., entropy and heat capacity). This however will not significantly affect our predictions for the pressures or the phase stability regions for the solutions.

The free energy for a hard-sphere fluid consists of two terms: the ideal gas free energy [F_{ig}], and an additional term corresponding to the hard-sphere interactions. For the second term, we have chosen to use the approximation for mixtures derived by Mansoori, et al. (1971), which can be written as:

$$F_{hs} = F_{ig} + T\,[-3/2\,(1-y_1+y_2+y_3) + (3y_2+2y_3)/(1-\eta) + 3/2\,(1-y_1-y_2-y_3/3)/(1-\eta)^2 + (y_3-1)\,\ln(1-\eta)\,, \qquad (5.4)$$

where

$$y_1 = D_{12}\,(d_1+d_2)/(d_1d_2)^{1/2}\,,$$

$$y_2 = D_{12}\,[\eta_1\,(d_2/d_1)^{1/2} + \eta_2\,(d_1/d_2)^{1/2}]\,/\,\eta\,,$$

$$y_3 = [((1-x)(\eta_1)^2)^{1/3} + (x(\eta_2)^2)^{1/3}]^3\,/\,\eta^2\,,$$

$$D_{12} = [x(1-x)\eta_1\eta_2]^{1/2}\,(d_2-d_1)^2\,/\,(\eta d_1d_2)\,,$$

$$\eta_i = \pi x_i d_i^3\,/\,6v\,,$$

η ($=\eta_1+\eta_2$) is the hard-sphere packing fraction (defined as the ratio of the volume occupied by hard-spheres to the total volume), and d_i is the hard-sphere diameter of the i^{th} ion. This expression finds results for the mixing properties of binary systems which are in good agreement with those from molecular dynamics calculations.

The next term to be considered is the Coulomb energy for a two-component-plasma. This is the electrostatic energy of ions

immersed in the uniform electron background, with the arrangement of ions in the fluid approximated by a Percus-Yevick hard-sphere distribution. The analytic expression for this term has been derived by Ross and Seale (1974), and used by Stevenson (1975). Minor errors exist in both papers. The correct expression for a mixture with effective ion charges Z_1^* and Z_2^* is:

$$W = -3\eta^{2/3}/[5r_s(1+2\eta)]\left[\alpha^2(1-x)^2(Z_1^*)^2G_{11} + \frac{1}{2}(1-\alpha)^2x(1-x)Z_1^*Z_2^*G_{12} + x^2(Z_2^*)^2G_{22}\right], \quad (5.5)$$

where

$$G_{11} = \eta_1^2 - 2\eta_1 + 10 - 4\eta_1\eta_2 + 10\eta_2 + 10(\eta_1\eta_2-\eta_2)/\alpha + (\eta_2^2-2\eta_2-4\eta_1\eta_2)/\alpha^2 ,$$

$$G_{12} = 30(\eta_1-\eta_2)(1-\alpha)/(1+\alpha) - 30(1+\eta) + (2\alpha/(1+\alpha))^2[\eta_1^2-2\eta_1+10-4\eta_1\eta_2+20\eta_2 +10(\eta_1\eta_2+\eta+2)/\alpha + (\eta_2^2-2\eta_2+10-4\eta_1\eta_2+20\eta_1)/\alpha^2],$$

$\alpha = d_1/d_2$, and G_{22} is found from G_{11} by substituting η_2 for η_1 and α for $1/\alpha$.

Finally, the first-order quantum correction for a hard-sphere system has been included. This was derived by Jancovici (1969) and has the form:

$$F_{qm} = T\frac{3}{4r_s^3}\left[\frac{\pi}{T}\right]^{1/2}[(1-x)^2g_{11}d_1^2m_{11}^{1/2} + 2x(1-x)g_{12}d_{12}^2m_{12}^{1/2} + x^2g_{22}d_2^2m_{22}^{1/2}] \text{ au/ion}, \quad (5.6)$$

where

$$\frac{1}{m_{ij}} = \frac{1}{m_i} + \frac{1}{m_j} ,$$

$$d_{12} = d_1 + d_2 ,$$

m_i is the mass of the i^{th} ion (in electron masses), and g_{ij} is the classical pair-correlation function evaluated at the hard-sphere surfaces (see e.g., Lebowitz, 1964). Eq. (5.6) represents a series expansion in powers of the thermal wavelength $\lambda = (2\pi\hbar^2/mk_BT)^{1/2}$, which will rapidly converge provided $\lambda << d$. At densities we are considering ($r_s \sim d \sim 1$), this condition is satisfied when $T >> 1000^oK$. Note also that the first-order quantum correction for the hard-sphere system is $\sim \hbar$, whereas the first term in the Wigner-Kirkwood expansion is $\sim \hbar^2$. This is because the terms for the Wigner-Kirkwood expansion diverge for the case of the hard-sphere potentials, which are non-analytic (Jancovici, 1969).

The free energies of the first-order quantum correction are small ($\sim 10^{-2}$ au/ion), and did not significantly affect our results for the pressures or mixing energies. Its effects are more strongly felt for the entropy and heat capacity, especially at lower temperatures, where presumable higher-order terms become important.

CHAPTER 6

RESULTS FOR FLUID MIXTURES

H-He Mixtures

For specified values of the density, temperature, and composition, the free energies are determined by minimizing the last three terms in eq. (5.1) as a function of α and η, and then adding the structure-independent terms F_e and E_{si}. The derivatives of the free energy (e.g., pressure, entropy) are evaluated numerically. The value of α for H-He solutions is found to have a rather weak dependence on r_s, T, and x, and generally lies within the range of 0.76-0.80. The hard-sphere packing fraction [η] is of course more sensitive to these variables.

The primary purpose of this study is to estimate the temperatures at which mixtures become unstable to phase separation based on the TFD model. To do this, we first evaluate the Gibbs energy in (T,P,x) space. The stability condition we have used is:

$$[\partial^2 G/\partial x^2]_{T,P} < 0 . \qquad (6.1)$$

Though this condition does not exactly reproduce the same temperatures along the phase separation curve as the "common tangent" method, except at the critical temperature [i.e., the maximum temperature along the curve] (see e.g., Broecker and Oversby, 1971), it is a very

efficient method for estimating the phase stability of mixtures near critical temperatures. The LHS of eq. (6.1) is most easily evaluated by calculating the Gibbs energy at 3 closely spaced compositions for a constant temperature and pressure, and numerically differentiating.

The stability condition was tested for a number of different temperatures and compositions at our pressures of interest. At 10, 100, and 1000 Mbar, the critical temperatures for H-He solutions were found to be $\sim 0^{o}K$, $500^{o}K$, and $1500^{o}K$, respectively. At these relatively low temperatures, the hard-sphere packing fractions were found to be ~ 0.5 to 0.6, exceeding the solidification value of $\eta \sim 0.45$ for classical liquids. Therefore, based on the hard-sphere model and Thomas-Fermi-Dirac theory, one might expect H-He mixtures to be stable against phase separation at all temperatures above the melting temperatures. But using this approach to estimate the freezing curve for metallic hydrogen is very questionable. Although this freezing criterion [$\eta \sim 0.45$] has been shown to be fairly accurate for H_2 and He at pressures $\lesssim 10^5$ Mbar (Young and Ross, 1981; Young, et al., 1981), detailed theoretical studies at higher pressures indicate that metallic hydrogen may be stable in the liquid phase even at $T = 0^{o}K$ (Chakravarty and Ashcroft, 1979).

The phase separation temperatures found using our TFD pseudopotentials are considerably lower ($\sim$ 6000 to $10000^{o}K$) than those found using free electron perturbation theory (Stevenson, 1975). This result is not unexpected. Solid-state calculations at $T = 0^{o}K$ have shown that TFD mixing energies are typically $\sim 0.01 - 0.02$ au/ion

lower than those found using linear response theory (see Chapter 3). This suggests that the TFD phase separation temperatures should be $\sim$ 0.02 - 0.04 au (or $\sim$ 6000 to 12000°K) lower than the linear response temperatures because the phase separation temperatures depend on the second derivative of the Gibbs energy with respect to composition. Our critical temperatures are also lower than those found for the two-component-plasma model (Hansen and Vieillefosse, 1976) and the linear response model using the Yukawa potential (Firey and Ashcroft, 1977), although both of these models predict somewhat lower critical temperatures than Stevenson's.

Such diverse predictions for the phase stability regions of H-He solutions make it difficult to theoretically predict with any confidence whether this process is currently playing a major role in the energy balance of Saturn. At a pressure of $\sim$ 10 Mbar, Saturn is expected to have a temperature of $\sim$ 8000°K (Hubbard, et al., 1980). If the phase separation temperatures for H-He solutions near this pressure are $\gtrsim$ 8000°K, we should expect He-rich and He-poor phases to form, with the denser He-rich phase sinking toward the center of the planet. Our TFD results predict that this process should not be occuring in either Jupiter or Saturn at the present time.

We have also calculated other equilibrium properties based on TFD theory and our model free energy for the liquid state. The equations of state for pure hydrogen and pure helium have been computed along 2 isotherms, and fitted to the following polynomial:

$$P = 51.6\, s^{-5} [1 + u_1 s + u_2 s^2 + u_3 s^3] \text{ Mbar} , \qquad (6.2)$$

where u_1, u_2, and u_3 are constants listed in Table 10 for isotherms at 6000°K and 15000°K, and s is the electron spacing parameter now defined using the actual ion charges. Pressures at other temperatures can be estimated by linear interpolation. The pressures for H-He mixtures can be determined using the "additive volume" rule, which should be quite accurate because the volumetric deviations from ideal mixing are small [$\delta V/V \lesssim 0.1$ %].

The equation of state for hydrogen does not differ significantly from that determined from linear response theory. However, the TFD pressures for helium are $\sim$ 20-25 % higher. Because it is questionable whether the free electron perturbation expansion converges sufficiently for a He atom, the TFD equation of state for He may be somewhat more reliable. The TFD pressures for helium also agree relatively well with those determined from linear-muffin-tin-orbital calculations (Young, et al., 1981).

We have also evaluated the entropy at a few points of interest. For $x = 0$, $r_s = 0.9$, and $T = 35000$°K, we find an entropy of $S = 7.92\, Nk_B$ (k_B = Boltzmann's constant). This is somewhat smaller that the values obtained by Stevenson [$S = 8.55 Nk_B$] and by DeWitt and Hubbard (1976) [$S = 8.22 Nk_B$]. Our relatively low entropies would predict central temperatures for Jupiter higher by 3000 to 6000°K than the other values. These results can also be compared to the entropy for the TCP model [$S = 7.41 Nk_B$, using hard-sphere perturbation

Table 10

Parameters for H-He Equations of State

Ion	T(°K)	u_1	u_2	u_3
H	6000	-0.5586	-0.0014	+0.0730
H	15000	-0.5546	+0.0586	+0.0757
He	6000	-0.8723	+0.2096	+0.0164
He	15000	-0.8700	+0.2465	+0.0170

theory], and that of an ideal gas [$S = 8.82Nk_B$]. Note that the lower entropies indicate a greater thermal dependence on the non-ideal part of the free energy.

The larger thermal dependence for the TFD model is also reflected in the heat capacities. For $x = 0$, $r_s = 0.9$, and $T = 20000^oK$, we find a heat capacity of $C_V = 2.4Nk_B$, compared with the lower values from Stevenson [$C_V = 1.8Nk_B$] and Hubbard (1972) [$C_V = 1.9Nk_B$]. The result for the TCP model is $C_V = 2.6Nk_B$, and an ideal gas of course has $C_V = 1.5Nk_B$.

There are two possibilities for the larger temperature dependence on our model free energy. First, the structure-independent free energy term determined from the solid-state TFD results contains no thermal contribution, and therefore cannot aid in reducing $[dF/dT]_V$. The second possibility, which is more likely, is that the hard-sphere pair-distribution functions do not adequately approximate the actual pair-distribution functions (as Monte Carlo results do). Though Stevenson also based his calculations on hard-sphere perturbation theory, he effectively converted to a more realistic pair-distribution function by including a correction term based on the optimized-random-phase-approximation of Andersen, et al. (1972). Even though this correction is small (Stevenson, 1975), it is large enough to significantly affect results for the entropy.

H-C and H-O Mixtures

Similar calculations were carried out for fluid H-C and H-O solutions based on the TFD model and hard-sphere perturbation theory. The phase separation temperatures were again found using eq. (6.1), with the results being summarized in Table 11. For H-C solutions, the critical temperatures were found to be roughly 0, 1000, and 8000 ^{o}K at pressures of 10, 100, and 1000 Mbar, while for H-O solutions, the critical temperatures were roughly 0, 0, and 10,000 ^{o}K, respectively. Because of larger errors present in the fits to the solid-state data for the H-C and H-O mixtures, the errors in the critical temperatures are $\sim$ a few thousand degrees.

The TFD phase separation temperatures are much lower than their TCP counterparts. Stevenson (1976) has estimated the TCP critical temperatures to be $\sim 1.1 \times 10^5$ ^{o}K and $\sim 2.6 \times 10^5$ ^{o}K for the H-C and H-O systems, respectively. The lower TFD temperatures are not unexpected however, because the TFD mixing energies for the solid-state computations were typically $\sim$ 1 au/ion ($\sim 3 \times 10^5$ ^{o}K) lower than their TCP counterparts (Chapter 3).

Whether or not carbon and oxygen are soluble in metallic hydrogen at pressures of 10 to 100 Mbar may have important consequences for the chemical distributions and energy balances of Jupiter and Saturn. If either atom is immiscible in the metallic zone, the denser material could sink toward the central core of the planet, and should deplete the upper atmosphere of that species.

Table 11

Critical Temperatures for H-He, H-C, and H-O Solutions

Pressure (Mbar)	T_{H-He}	T_{H-C}	T_{H-O}
10	0 °K	0 °K	0 °K
100	500 °K	1000 °K	0 °K
1000	1500 °K	8000 °K	10000 °K

Although carbon is observed to be present in roughly solar proportions in the atmospheres of Jupiter and Saturn, oxygen (in the form of H_2O) seems to be significantly depleted in Jupiter (Bjoraker, 1983). The immiscibility of H-O solutions may be responsible for this depletion of oxygen, although our TFD results do not suggest this. It is noted, however, that qualitatively oxygen tends to mix less readily than carbon with hydrogen at high pressures.

The pressure-density relations for fluid H-C and H-O mixtures have been evaluated and fitted to eq. (6.2). Along an isotherm of $T = 10{,}000\ ^{o}K$, the constants in eq. (6.2) are given by:

$$u_i = \sum_{j=1}^{4} w_{ij}\, x^{j-1} , \qquad (6.3)$$

where x is the number fraction of the larger ion, and w_{ij} are constants given in Table 12. The above expression is valid for pressures of 10 to 10^3 Mbar and reproduces the TFD results to $\lesssim$ 1%. Pressures at other temperatures can be found using other tables in this section.

As noted earlier, the TFD model tends to predict lower energies and higher pressures than the actual values. This is also the case for H-O mixtures. High pressure equations of state for H_2O are often based on interpolation between low pressure experimental data and the TFD model at high pressures. Though the H_2O equation of state will approach the TFD curve in the high pressure limit ($r_s \to 0$), experimental results (Mitchell and Nellis, 1979) indicate that for pressures near 1 Mbar, the TFD pressures are $\sim$ 50% too large.

Tables 12

Parameters for H-C and H-O Equations of State

Mixture	i \ j	1	2	3	4
H-C:	1	-0.591	-3.720	+4.675	-1.963
	2	+0.091	+2.693	-2.219	+0.247
	3	+0.039	-0.477	-0.413	+0.808
H-O:	1	-0.600	-5.378	+7.643	-3.653
	2	+0.097	+4.833	-6.248	+2.838
	3	+0.040	-1.376	+1.534	-0.632

Other thermodynamic properties of fluid solutions can also be readily evaluated using hard-sphere perturbation theory. Listed in Tables 13 and 14 are the entropies [S/Nk_B] for the H-C and H-O mixtures, respectively. The entropies were computed for a number of temperatures [T], compositions [x], and electron spacing parameters [s; defined using the actual ion charges]. As noted in discussing the results for H-He solutions, the entropies found using the hard-sphere distribution function tend to overestimate the thermal dependence of the non-ideal gas contribution to the free energy. Therefore, the tabulated entropies are probably somewhat low, and the actual values should lie somewhere between our results and the values calculated for an ideal gas.

Listed in Tables 15 and 16 are the heat capacities [C_V/Nk_B] for the H-C and H-O systems determined from hard-sphere calculations over the same (s,T,x)-space. The heat capacity for a high temperature Debye solid is $C_V = 3.0\ Nk_B$, and that for an ideal monatomic gas is of course $C_V = 1.5\ Nk_B$. The results for a liquid are generally somewhere between these two values. As seen in the tables, the heat capacities are somewhat high and are commonly greater than the value for a high temperature solid. This again is a consequence of the large thermal contribution to the hard-sphere free energy.

Finally, the Gruneisen parameters have been computed and are listed in Tables 17 and 18. This quantity is given by:

$$\gamma = [\partial \ln(T)/\partial \ln(\rho)]_S = V\,(\partial P/\partial T)_V\,/C_V, \qquad (6.4)$$

Table 13

Entropies $[S/Nk_B]$ for H-C Mixtures

	$T(^oK)$ \ x	0.00	0.25	0.50	0.75	1.00
s = 0.6:	10,000	2.75	4.06	4.62	4.80	4.48
	15,000	3.93	5.35	6.03	6.33	6.13
	24,000	5.19	6.73	7.53	7.96	7.89
	35,000	6.14	7.76	8.66	9.18	9.20
s = 0.8:	10,000	4.26	5.88	6.72	7.17	7.13
	15,000	5.34	7.04	7.97	8.51	8.56
	24,000	6.51	8.30	9.32	9.96	10.11
	35,000	7.40	9.26	10.36	11.07	11.29
s = 1.0:	10,000	5.41	7.25	8.29	8.93	9.06
	15,000	6.42	8.32	9.43	10.14	10.35
	24,000	7.53	9.50	10.68	11.47	11.76
	35,000	8.37	10.40	11.65	12.51	12.96

Table 14

Entropies $[S/Nk_B]$ for H-O Mixtures

	T(°K) \ x	0.00	0.25	0.50	0.75	1.00
s = 0.6:	10,000	2.75	4.22	4.79	4.95	4.61
	15,000	3.93	5.53	6.23	6.54	6.34
	24,000	5.19	6.92	7.78	8.23	8.18
	35,000	6.14	7.97	8.94	9.50	9.56
s = 0.8:	10,000	4.26	6.12	7.03	7.53	7.53
	15,000	5.34	7.29	8.31	8.91	9.01
	24,000	6.51	8.56	9.69	10.40	10.62
	35,000	7.40	9.52	10.74	11.55	11.84
s = 1.0:	10,000	5.41	7.54	8.69	9.41	9.62
	15,000	6.42	8.61	9.84	10.65	10.94
	24,000	7.53	9.80	11.12	12.01	12.40
	35,000	8.37	10.71	12.11	13.08	13.54

Table 15

Heat Capacities [C_v/Nk_B] for H-C Mixtures

	$T(^oK)$ \ x	0.00	0.25	0.50	0.75	1.00
s = 0.6:	10,000	3.04	3.32	3.63	3.94	4.26
	15,000	2.80	3.06	3.34	3.63	3.91
	24,000	2.57	2.82	3.08	3.33	3.59
	35,000	2.43	2.67	2.91	3.15	3.39
s = 0.8:	10,000	2.76	2.96	3.19	3.39	3.66
	15,000	2.58	2.77	2.99	3.15	3.42
	24,000	2.41	2.60	2.80	2.92	3.20
	35,000	2.30	2.49	2.69	2.77	3.08
s = 1.0:	10,000	2.57	2.72	2.89	3.08	3.26
	15,000	2.43	2.57	2.74	2.91	3.09
	24,000	2.29	2.44	2.61	2.78	2.95
	35,000	2.21	2.37	2.54	2.72	2.89

Table 16

Heat Capacities [C_v/Nk_B] for H-O Mixtures

	T(°K) \ x	0.00	0.25	0.50	0.75	1.00
s = 0.6:	10,000	3.04	3.36	3.72	4.10	4.47
	15,000	2.80	3.10	3.43	3.77	4.11
	24,000	2.57	2.86	3.16	3.47	3.77
	35,000	2.43	2.71	2.99	3.28	3.57
s = 0.8:	10,000	2.76	2.98	3.24	3.51	3.79
	15,000	2.58	2.79	3.04	3.29	3.54
	24,000	2.41	2.62	2.85	3.09	3.32
	35,000	2.30	2.52	2.75	2.98	3.20
s = 1.0:	10,000	2.57	2.72	2.92	3.13	3.34
	15,000	2.43	2.58	2.77	2.97	3.17
	24,000	2.29	2.45	2.65	2.85	3.05
	35,000	2.21	2.38	2.60	2.81	3.01

Tables 17

Gruneisen Parameters [γ] for H-C Mixtures

	T(°K) \ x	0.00	0.25	0.50	0.75	1.00
s = 0.6:	10,000	0.58	0.65	0.69	0.72	0.74
	15,000	0.59	0.65	0.69	0.71	0.74
	24,000	0.59	0.65	0.68	0.71	0.73
	35,000	0.60	0.65	0.68	0.71	0.72
s = 0.8:	10,000	0.62	0.70	0.75	0.79	0.81
	15,000	0.63	0.70	0.74	0.79	0.80
	24,000	0.63	0.69	0.73	0.78	0.79
	35,000	0.63	0.69	0.72	0.78	0.77
s = 1.0:	10,000	0.67	0.75	0.80	0.83	0.86
	15,000	0.67	0.74	0.78	0.82	0.85
	24,000	0.67	0.73	0.77	0.80	0.82
	35,000	0.66	0.72	0.76	0.78	0.80

Table 18

Gruneisen Parameters [γ] for H-O Mixtures

	T(°K) \ x	0.00	0.25	0.50	0.75	1.00
s = 0.6:	10,000	0.58	0.67	0.72	0.76	0.79
	15,000	0.59	0.67	0.72	0.75	0.78
	24,000	0.59	0.67	0.71	0.74	0.77
	35,000	0.60	0.67	0.71	0.74	0.76
s = 0.8:	10,000	0.62	0.72	0.78	0.82	0.86
	15,000	0.63	0.72	0.77	0.81	0.84
	24,000	0.63	0.71	0.76	0.80	0.82
	35,000	0.63	0.71	0.75	0.78	0.81
s = 1.0:	10,000	0.67	0.77	0.83	0.87	0.90
	15,000	0.67	0.76	0.81	0.85	0.88
	24,000	0.67	0.75	0.79	0.82	0.85
	35,000	0.66	0.74	0.77	0.80	0.82

where ρ is the mass density. For an ideal gas, γ would be 2/3 and for a high temperature solid, γ would be 0.5. Again, the thermal dependence of the hard-sphere interaction appears to be too large, especially for the larger ions.

CHAPTER 7

CONCLUSIONS AND DISCUSSION

Summary of Results

The purpose of this study has been twofold. The first has been to determine whether the phase separation temperatures for H-He mixtures found using free electron perturbation theory are confirmed by the Thomas-Fermi-Dirac model. The second has been to develop a more realistic approach to computing the high pressure mixing properties of systems containing many-electron atoms than either the two-component-plasma model or perturbation theory.

In regards to the former, it is clear that our TFD results for H-He solutions do <u>not</u> confirm those found from Stevenson's perturbation theory approach. The TFD critical temperatures are 6,000 to 10,000 ^{o}K lower at pressures $\lesssim 10^{3}$ Mbar and suggest that fluid H-He solutions should be stable against phase separation down to temperatures $\lesssim$ 1500 ^{o}K. Because these temperatures are much lower than those found in the metallic zones of Jupiter and Saturn, our TFD results suggest that helium is soluble in metallic hydrogen in each of these planets and therefore, gravitational energy due to phase separation should not be contributing to the energy budgets of either of these planets.

For systems containing many-electron atoms, we have found the phase separation temperatures for H-C and H-O solutions to be much lower than their TCP values. Because the TFD critical temperatures for pressures $\lesssim$ 100 Mbar are so low ($\lesssim 10^3$ ^oK), the TFD results suggest that carbon and oxygen should also be soluble in the metallic zones of Jupiter and Saturn. At pressures near 1000 Mbar, the critical temperatures for H-C and H-O solutions are roughly 8,000 and 10,000 ^oK, respectively. Although this pressure is greater than the central pressures in Jupiter and Saturn, it is worth noting that qualitatively the critical temperatures for the H-O solutions rise more rapidly with pressure than the H-C solutions.

The Stability of Solutions at High Pressure

The question of whether or not He is immiscible in metallic hydrogen at temperatures and pressures representative of giant planetary interiors is an important one which has not yet been resolved. Calculations based on Thomas-Fermi-Dirac theory find critical temperatures significantly lower than those found using free electron perturbation theory. Though the results from these theories do not differ drastically for thermodynamic properties such as the total energy and pressure, small but very significant differences arise in the mixing energies, leading the very different predictions for the phase stability regions of H-He solutions. And as was found from solid-state calculations (Chapter 3), these differences in the mixing energies persist up to very high pressure ($P >> 10^6$ Mbar).

We do not expect the TFD results for H-He solutions to be more reliable than those from linear response calculations. Deficiencies in the TFD model have been discussed here (Chapter 2) and in other sources (see e.g., Landau and Lifshitz, 1965). Though the TFD model is somewhat crude, it does provide an alternative, non-linear approach to evaluating the mixing properties of binary systems, and as we have shown, can be used for systems containing many-electron atoms, where free electron perturbation theory breaks down.

In this study, we have shown that predicting the phase stability regions of high pressure H-He fluids is rather model-dependent. In light of this, it is questionable whether the immiscibility of helium in metallic hydrogen is responsible for the anomalously high luminosity of Saturn. This question, however, could ultimately be resolved by accurate measurements of the H_2/He ratio in the upper atmospheres of Jupiter and Saturn. Because heat from the deep interiors of the Jovian planets is being transported by convection (up to pressures near 1 bar), the chemical constituents throughout the predominantly hydrogen regions should be well mixed. Therefore, in the absence of H-He phase instabilities in the metallic zones, the H/He ratios in Jupiter and Saturn should be the same (both being equal to the solar H/He ratio).

Though spacecraft observations seem to support a depletion of helium in Saturn's atmosphere, the results are not conclusive. The H_2 mole fraction [$x(H_2)=N(H_2)/(N(H_2)+N(He))$] in the upper atmosphere of Jupiter has been inferred to be 0.88 ± 0.06 from Pioneer (Orton and

Ingersoll, 1976) and 0.90 ± 0.03 from Voyager (Gautier, et al., 1981). The H_2 mole fraction in Saturn's atmosphere was found to be 0.90 ± 0.03 from Pioneer (Orton and Ingersoll, 1980) and 0.94 ± 0.03 from Voyager (Hanel, et al., 1981). The larger H_2 mole fraction found from the Voyager observations tend to suggest helium is depleted in Saturn's upper atmosphere (implying a He-rich zone near the central core), but the uncertainties are still too large to be conclusive. Sending probes into the atmospheres of Jupiter and Saturn should provide more accurate determinations of their helium abundances.

The instability of carbon or oxygen in metallic hydrogen may also play an important role in the energy balances of Jupiter and Saturn. This is especially true for Saturn because volatile species such as CH_4 and H_2O may have been able to condense in the formation region of Saturn, but would have been less likely to condense in the warmer formation region of Jupiter. Because material which was able to condense in the formation region of a giant planet is expected to be enhanced in its interior (Hubbard and MacFarlane, 1980), carbon and oxygen may represent a larger fraction of the mass of Saturn relative to Jupiter. In addition, interior models (Hubbard, et al., 1980) indicate the relative abundance of "core material" (composed of species able to condense in the formation region of a planet) is greater for Saturn (representing $\sim$ 20% of its total mass) than Jupiter ($\sim$ 5% of the total mass). For instance, the total mass of oxygen in Saturn may be as high as 8-10 Earth masses, compared to 13-15 Earth masses of helium. Thus, carbon and oxygen, because of their greater

relative abundances, may play a more important role in the thermal history of Saturn.

Infrared observations seem to indicate the C/H ratios for both Jupiter and Saturn are roughly 2 to 3 times greater than the solar value (Gautier, et al., 1982; Encrenaz and Combes, 1982). Although these enrichments of carbon could indicate than CH_4 had condensed in regions where their protoplanetary cores formed, it seems more likely that the enrichment, if it actually exists, could be due to the late accretion of planetesimals from the outer regions of the solar system (Hubbard and Stevenson, 1983). In any case, the observations are consistent with a roughly solar abundance of carbon (relative to hydrogen), with the carbon being uniformly distributed throughout the predominantly hydrogen regions of the planets.

Although no results are available on the oxygen abundance in Saturn, H_2O has been detected in Jupiter from 5μ observations (Larson, et al., 1975). Recent analysis of Voyager data (Bjoraker, 1983) finds that H_2O may be depleted in the atmosphere of Jupiter by a factor of 10^2 to 10^3 relative to the solar value. This suggests that oxygen may be trapped in the deep interior of Jupiter, perhaps surrounding the dense silicate core. If this is the case, one can only speculate as to the abundance of oxygen in Jupiter. But more important, this raises the question of whether oxygen is soluble in the metallic zone of Jupiter.

If H-O solutions become immiscible in the deep interior of Jupiter, the denser oxygen-rich phase could become trapped at the base

of the metallic zone, resulting in a depletion of oxygen in the observable atmosphere. Moreover, because Saturn's internal temperatures are lower than Jupiter's, H-O mixtures would also be expected to be unstable in the deep interior of Saturn. If H-O solutions are indeed unstable to phase separation, and if the process of separation is presently occurring (or has occurred during the past 2 billion years), it is possible that H-O (and not H-He) immiscibility may be responsible for Saturn's excess luminosity.

The above scenario is clearly speculative, but it is not qualitatively inconsistent with our Thomas-Fermi-Dirac results, since the TFD critical temperatures tend to be higher for H-O mixtures. However, it must be emphasized that for a particular mechanism to be responsible for Saturn's current excess energy output, it must have been contributing energy at some point during the past 2 billion years (Pollack, et al., 1977). Therefore, if hydrogen-oxygen mixtures separated early in Saturn's history, it could not account for Saturn's excess luminosity.

Future Work

The approach of using hard-sphere perturbation theory with pseudopotentials derived from solid-state Thomas-Fermi-Dirac calculations can also be used to study other mixtures. Investigating the mixing properties of iron-sulfur and iron-oxygen solutions may provide help in predicting the composition of the Earth's outer liquid

core. Also, a study of the carbon-oxygen system may provide results relevant to the interiors of white dwarfs.

It should be noted, however, that some improvements need to be made in the pseudopotentials if the mixing properties of high-Z solutions are to be determined to an accuracy where significant predictions can be made for planetary interiors. Currently, the errors introduced in fitting the pseudopotentials to the solid-state TFD data are the main source of error. As stated in Chapter 6, these errors lead to uncertainties in the H-C and H-O critical temperatures of $\sim$ a few x 10^{o}K. For even higher-Z mixtures (e.g., Fe-S), uncertainties would likely be an order of magnitude larger. Therefore, it appears that a pseudopotential other than that based on the two-component-plasma potential will have to be used to better reproduce the solid-state data.

REFERENCES

Abramowitz M. and Stegun I. A. (1965) Handbook of Mathematical Functions, with Formulas, Graphs, and Mathematical Tables, New York, Dover.

Andersen H. C., Chandler D. and Weeks J. D. (1972) Roles of repulsive and attractive forces in liquids: the optimized random phase approximation. J. Chem. Phys. 56, 3812-3823.

Armstrong K. R., Harper D. A. Jr. and Low F. J. (1972) Far-infrared brightness temperatures of the planets. Astrophys. J. 178, L89-L92.

Bjoraker G. (1983) Private comm., Dept. of Planetary Sci., Univ. of Arizona.

Broecker W. S. and Oversby V. M. (1971) Chemical Equilibria in the Earth, New York, McGraw-Hill.

Brush S. G., Sahlin H. L. and Teller E. (1966) A Monte Carlo study of a one-component plasma. J. Chem. Phys. 45, 2102-2118.

Chakravarty S. and Ashcroft N. W. (1978) Ground state of metallic hydrogen. Phys. Rev. B18, 4588-4597.

DeWitt H. E. and Hubbard W. B. (1976) Statistical mechanics of light elements at high pressure. IV. A model free energy for the metallic phase. Astrophys. J. 205, 295-301.

Dyson F. J. (1971) Chemical binding in classical Coulomb lattices. Annals Phys. 63, 1-11.

Encrenaz T. and Combes M. (1982) On the C/H and D/H ratios in the atmospheres of Jupiter and Saturn. Icarus 52, 54-61.

Ewald P. P. (1921) Die berechnung optischer and elektrostatischer gitterpotentiale. Ann. Phys. 64, 253-287.

Fermi E. (1930) Eine statistische methode zur bestimmung einiger eigenschaften des atoms und ihre anwendung auf die theorie des periodischen systems der elemente. Z. Phys. 48, 73-79.

Feynman R. P., Metropolis N. and Teller E. (1949) Equations of state of elements based on generalized Thomas-Fermi theory. Phys. Rev. 75, 1561-1573.

Firey B. and Ashcroft N. W. (1977) Thermodynamics of Thomas-Fermi screened Coulomb systems. Phys. Rev. A15, 2072-2078.

Friedli and Ashcroft N. W. (1975) Aluminum under high pressure. I. Equation of state. Phys. Rev. B12, 5552-5559.

Gautier D., Bezard B., Marten A., Baluteau J. P., Scott N., Chedin A., Kunde V. and Hanel R. (1982) The C/H ratio in Jupiter from the Voyager infrared investigation. Astrophys. J. 257, 901-912.

Gautier D., Conrath B., Flaser M., Hanel R., Kunde V., Chedin A. and Scott N. (1981) The helium abundance of Jupiter from Voyager. J. Geophys. Res. 86, 8713-8720.

Graboske H. C. Jr., Pollack J. B., Grossman A. S. and Olness R. J. (1975) The structure and evolution of Jupiter: The fluid contraction phase. Astrophys. J. 199, 265-281.

Hanel R., Conrath B., Flasar F. M., Kunde V., Maguire W., Pearl J., Pirraglia J., Samuelson R., Herath L., Allison M., Cruikshank D., Gautier D., Gierasch P., Horn L., Koppany R. and Ponnamperuma C. (1981) Infrared observations of the Saturnian system from Voyager 1. Science 212, 192-200.

Hansen J. P. and Vieillefosse P. (1976) Equation of state of the classical two-component plasma. Phys. Rev. Lett. 37, 391-394.

Hubbard W. B. (1972) Statistical mechanics of light elements at high pressure. II. Hydrogen and helium alloys. Astrophys. J. 176, 525-531.

Hubbard W. B. (1980) Intrinsic luminosities of the Jovian planets. Rev. Geophys. Space Phys. 18, 1-9.

Hubbard W. B. and MacFarlane J. J. (1980) Structure and evolution of Uranus and Neptune. J. Geophys. Res. 85, 225-234.

Hubbard W. B., MacFarlane J. J., Anderson J. D., Null G. W. and Biller E. D. (1980) Interior structure of Saturn inferred from Pioneer 11 gravity data. J. Geophys. Res. 85, 5909-5916.

Hubbard W. B. and Slattery W. L. (1971) Statistical mechanics of light elements at high pressure. I. Theory and results for metallic hydrogen with simple screening. Astrophys. J. 168, 131-139.

Hubbard W. B. and Stevenson D. J. (1983) In preparation.

Jancovici B. (1969) Quantum-mechanical equation of state for a hard sphere gas at high temperature. Phys. Rev. 178, 295-297.

Landau L. D. and Lifshitz E. M. (1965) Quantum Mechanics, New York, Pergamon.

Landau L. D. and Lifshitz E. M. (1969) Statistical Physics, Reading, Mass., Addison-Wesley.

Larson H. P., Fink U., Treffers R. and Gautier T. N. (1975) Detection of water vapor on Jupiter. Astrophys. J. 197, L137-L140.

Lebowitz J. L. (1964) Exact solution of generalized Percus-Yevick equation for a mixture of hard spheres. Phys. Rev. A133, 895-899.

Low F. J. (1966) Observations of Venus, Jupiter, and Saturn at 20 microns. Astron. J. 71, 391.

Lowenstein R. F., Harper D. A. Jr. and Moseley H. (1977) The effective temperature of Neptune. Astrophys. J. 218, L145-L146.

Mansoori G. A. and Canfield F. B. (1969) Variational approach to the equilibrium thermodynamic properties of simple liquids. J. Chem. Phys. 51, 4958-4967.

Mansoori G. A., Carnahan N. F., Starling K. E. and Leland T. W. Jr. (1971) Equilibrium thermodynamic properties of the mixture of hard spheres. J. Chem. Phys. 54, 1523-1525.

Mitchell A. C. and Nellis W. J. (1979) Water Hugoniot measurement in range 30-220 GPa. High Pressure Sci. Technol. 1, 428-434.

Mizushima M. (1970) Quantum Mechanics of Atomic Spectra and Atomic Structure, New York, W. A. Benjamin.

Orton G. S. and Ingersoll A. P. (1976) In Jupiter (Ed. by T. Gehrels). Pioneer 10 and 11 and groundbased infrared data on Jupiter: The thermal structure and He-H_2 ratio, pp. 207-215 (Univ. of Arizona, Tucson).

Orton G. S. and Ingersoll A. P. (1980) Saturn's atmospheric temperature structure and heat budget. J. Geophys. Res. 85, 5871-5881.

Pollack J. B., Grossman A. S., Moore R. and Graboske H. C. Jr. (1977) A calculation of Saturn's gravitational contraction history. Icarus 30, 111-128.

Ross M. and Seale D. (1974) Perturbation approximation to the screened Coulomb gas. Phys. Rev. A9, 396-399.

Salpeter E. E. (1973) On convection and gravitational layering in Jupiter and in stars of low mass. Astrophys. J. 181, L83-L86.

Salpeter E. E. and Zapolsky H. S. (1967) Theoretical high-pressure equations of state including correlation energy. Phys. Rev. 158, 876-886.

Smoluchowski R. (1967) Internal structure and energy emission of Jupiter. Nature 215, 691-695.

Stevenson D. J. (1975) Thermodynamics and phase separation of dense fully ionized hydrogen-helium fluid mixtures. Phys. Rev. B12, 3999-4007.

Stevenson D. J. (1976) Miscibility gaps in fully pressure-ionized binary alloys. Phys. Letters 58A, 282-284.

Stevenson D. J. and Salpeter E. E. (1977) The dynamics and helium distribution in hydrogen-helium fluid planets. Astrophys. J. Suppl. 35, 239-261.

Thomas L. H. (1927) Proc. Camb. Phil. Soc. 23, 542.

Young D. A., McMahan A. K. and Ross M. (1981) Equation of state and melting curve of helium to very high pressure. Phys. Rev. B24, 5119-5127.

Young D. A. and Ross M. (1981) Theoretical calculation of thermodynamic properties and melting curves for hydrogen and deuterium. J. Chem. Phys. 74, 6950-6955.